Environ Monit Assess (2023) 195:1265
https://doi.org/10.1007/s10661-023-11887-2

RESEARCH

Understanding the origins of and influences on precipitation major ion chemistry on the Island of O‘ahu, Hawai‘i

Theodore Brennis · Nicole Lautze · Robert Whittier · Giuseppe Torri · Donald Thomas

Received: 23 May 2023 / Accepted: 16 September 2023

Abstract Precipitation is the primary groundwater source for the Island of O‘ahu, Hawai‘i, USA, and is an important source of terrestrial nutrients. Since Pacific Islands are particularly vulnerable to the impacts of climate change, they are important venues for studying the controls on and fluctuations in precipitation chemistry. Spatial variations in some of the dissolved rainfall ions can also be of value as natural geochemical tracers in examining surface and groundwater flow. This study collected and chemically analyzed bulk precipitation from 20 sites across the Island of O‘ahu approximately quarterly between April 2018 and August 2021. The new precipitation chemistry data were integrated with previously published precipitation data to characterize major ion composition and examine the atmospheric processes controlling inorganic ion deposition. Linear regression and multivariate analysis were used to quantify the relationships among major ions and to assess the impacts of various environmental and meteorological factors on precipitation chemistry. Ordinary kriging and inverse distance weighted interpolations were conducted to help visualize spatial variations in major ion deposition. The results clearly indicate that ocean sea spray is the primary driver of precipitation inorganic chemistry, with marine sea salt aerosols accounting for more than 90% of the measured ion load. However, they also show that various weather patterns and nutrient sources impact inorganic deposition. Most notably, upper atmospheric transport of Asian continental dust during Hawaiian wet seasons, Ca^{2+} from local sedimentary deposits, and anthropogenic K^{+} from agricultural activity appear to be substantial non-marine deposition sources. This study synthesizes data from multiple sources into the most spatially and topographically diverse precipitation collector network on O‘ahu to date. The findings from this effort help establish a baseline for assessing future fluctuations in inorganic ion deposition and lay important groundwork for examining connections between precipitation and groundwater chemistry within the study area.

Keywords Precipitation · Deposition · Chemistry · Hawai‘i · Inorganic

T. Brennis (✉) · N. Lautze · R. Whittier · G. Torri · D. Thomas
University of Hawai‘i at Mānoa, 2500 Campus Rd, Honolulu, HI 96822, USA
e-mail: ted.brennis@gmail.com

Introduction

Precipitation chemistry is linked to environmental and atmospheric processes and as such has been the focus of much research over the last several decades (Ghahremaninezhad et al., 2016; Hutchinson, 1954; Keresztesi et al., 2020; Pearson & Fisher, 1971; Shi et al., 2009). Evaporated moisture is chemically pure H_2O such that any additional chemical

Published online: 03 October 2023

constituents in precipitation reflect its journey through the atmosphere (Lewis, 1981; Mphepya et al., 2004; Xiao, 2016). The analysis of precipitation chemistry not only reflects current atmospheric processes but also provides a baseline from which we can gauge future changes due to natural processes, climate change or anthropogenic activity.

Precipitation chemistry studies abound in scientific literature, but such Hawai'i-focused research is sparser and predominantly focused on O and H isotopologues or as related to volcanic influences on the Island of Hawai'i (Harding & Miller, 1982; Miller & Yoshinaga, 1981; Scholl & Ingebritsen, 1995; Tachera et al., 2021). Precipitation chemistry studies on the more populous Hawaiian Islands have largely focused on using stable isotopologues of water to explore moisture cycling in the atmosphere, surface waters, and subsurface hydrogeology (Booth et al., 2021; Dores et al., 2020; Glenn et al., 2013; Scholl et al., 2002; Torri et al., 2023). In the greater Pacific region, precipitation chemistry studies have been an effective tool to isolate nutrient contributions from anthropogenic, marine, and terrestrial sources (Li et al., 2007; Lu et al., 2011) and to illuminate key atmospheric processes, such as atmospheric wind regimes (Darzi & Winchester, 1982; Saltzman et al., 1986; Torri et al., 2023) and acid rain production (Lee et al., 2000; Satake & Yamane, 1992; Scholl & Ingebritsen, 1995). These and many other studies demonstrate the utility of assessing the relative abundances of chemical constituents in precipitation and stimulate a desire for more precipitation chemistry research in Hawai'i.

This paper presents inorganic ion data from bulk precipitation samples collected at 20 sites in and around the Pearl Harbor aquifer, on the island of O'ahu, Hawai'i, USA, approximately quarterly between April 2018 and August 2021. We incorporate data from previous work (Dores et al., 2020) to increase sample point density (Table 1; Fig. 1). Inorganic constituents in precipitation include ions that do not incorporate carbon into their chemical structure. While nitrogen-based compounds are commonly included in this category, we exclude them from the analysis due to source differentiation and biochemical reactivity uncertainties. In this study, the term "inorganics" refers to four major cations (Ca^{2+}, Mg^{2+}, K^{+}, Na^{+}) and two major anions (Cl^{-} and SO_4^{2-}).

The objective of this paper is to investigate inorganic ion deposition variability to characterize precipitation chemistry in and around the Pearl Harbor aquifer and to consider the atmospheric processes impacting changes in compositions over our collection period. Results from this study will lay groundwork for analyses of future fluctuations in precipitation chemistry in response to evolving climate change processes occurring in the North Pacific basin.

There are three dominant sources of inorganic ions in precipitation: terrestrial (crustal) dust, marine sea salt aerosols (SSAs), and anthropogenic activity. Terrestrial dust particles accumulate in the atmosphere through weathering of rocks and aeolian transport (Keresztesi et al., 2020; Pearson & Fisher, 1971); sea salt aerosols are formed when bubbles produced by breaking waves rise to the surface and burst, releasing microscopic aerosol particles which are transported by air currents (Keene et al., 1986; Laskin et al., 2012; Lewis & Schwartz, 2004); and anthropogenic sources of atmospheric inorganic particulates include a great variety of activities with the most massive sources being combustion of fossil fuels, industrial processes, and agriculture (Keresztesi et al., 2020; Lu et al., 2011; Pearson & Fisher, 1971). Hawai'i is one of a relatively small number of regions in which volcanic aerosols can also make substantial, localized contributions to the ion content of rainfall (Tachera et al., 2021). Chemical constituents can be delivered to the surface through both wet and dry deposition (Manahan, 2017); wet deposition occurs when chemically laden moisture precipitates and falls to the surface, where it can infiltrate the soil, be stored in the canopy, or be transported through runoff and throughfall processes; dry deposition occurs when suspended solid particulate matter settles on the surface. Dry deposition migrates along the ground surface through aeolian transport until it is arrested through either chemical, hydrologic, or physical means. Many processes can further impact both the speciation and the concentration of inorganic ions in atmospheric moisture during transport, such as biogenic activity (Ghahremaninezhad et al., 2016; Nightingale et al., 2000; Norman et al., 1999), acid–base reactions (Laskin et al., 2012 and references therein), and hygroscopicity (Hu et al., 2010, 2011). A more detailed review of these and other processes is included in the supplemental materials (Appendix). Simply put, no major ion is completely conservative, and the strength of the

Table 1 Summary of precipitation collector locations sampled between March 2017 and August 2021 on Oʻahu, Hawaiʻi, USA. Universal Transverse Mercator (UTM) zone is 4Q. Collectors with abbreviations beginning with "D" are from Dores et al. (2020)

Location Description	Abbreviation	*n*	Sample window	UTM Easting	UTM Northing	Latitude	Longitude	Elevation (ft)	Elevation (m)
Kaala Gate 3	K1	11	12/18–4/21	586,972	2,382,274	21.54118	−158.16010	953	290
Kaala Milepost 3	K2	9	7/19–4/21	586,483	2,381,009	21.52963	−158.16487	1813	553
Kaala Culvert 49	K3	9	7/19–4/21	587,231	2,379,032	21.51185	−158.15778	3051	930
Kaala Summit	KS	11	12/18–4/21	588,665	2,378,648	21.50827	−158.14395	3975	1212
Manana Trailhead	MT1	15	6/17–4/21	610,053	2,370,120	21.43008	−157.93803	956	291
Manana Trail 2	MT2	9	5/19–4/21	612,935	2,371,499	21.44235	−157.91015	1483	452
Manana Trail 3	MT3	9	5/19–4/21	614,505	2,372,110	21.44780	−157.89497	1801	549
Manana Trail Summit	MTS	7	7/19–4/21	616,531	2,373,121	21.45677	−157.87535	2644	806
Ewa Beach	EB	12	7/19–5/21	600,025	2,357,418	21.31592	−158.03555	24	7
Tripler Ridge	TR	12	7/19–4/21	617,134	2,363,592	21.37067	−157.87018	1247	380
Mililani High School	MHS	1	10/19–1/20	602,746	2,372,839	21.45508	−158.00838	727	222
Makakilo	M	10	10/19–5/21	594,714	2,363,528	21.37140	−158.08641	1099	335
Puu Waiawa LZ	PW	1	10/19–1/20	614,537	2,374,421	21.46866	−157.89450	2222	677
Kolekole Pass	KK	6	2/20–4/21	592,178	2,374,817	21.47352	−158.11030	1827	557
Schofield Barracks	SB	4	2/20–1/21	593,399	2,376,482	21.48850	−158.09840	1216	371
Wheeler Army Airfield	WAAF	5	2/20–4/21	599,238	2,375,874	21.48269	−158.04210	886	270
East Range	ER	5	2/20–4/21	603,095	2,376,433	21.48753	−158.00480	1004	306
Aiea	A	22	3/19–6/21	610,581	2,364,529	21.37949	−157.93322	43	13
Dept. of Health	DOH	33	4/18–8/21	609,043	2,368,670	21.41723	−157.94814	505	154
Waimanu Upper	WU	25	6/19–8/21	610,936	2,369,743	21.42663	−157.92957	1083	330
Kamehameha Hwy	D1	2	10/17–3/18	621,325	2,373,115	21.45642	−157.82910	20	6
Ewa Waimano	D3	5	4/17–7/18	610,052	2,370,111	21.43000	−157.93810	955	291
Haleiwa Wells	D4	2	10/17–3/18	593,961	2,386,342	21.57754	−158.09240	210	64
Hawai ʻi Ag. Center	D6	5	4/17–7/18	628,197	2,362,396	21.35911	−157.76360	364	111
HIG UH Mānoa	D7	5	4/17–7/18	622,760	2,355,609	21.29818	−157.81650	72	22
Honolulu F.R	D8	1	4/17–6/17	618,954	2,365,377	21.38667	−157.85250	617	188
Hoʻomaluhia B.G	D9	5	4/17–7/18	623,417	2,365,502	21.38750	−157.80940	213	65

Table 1 (continued)

Location Description	Abbreviation	*n*	Sample window	UTM Easting	UTM Northing	Latitude	Longitude	Elevation (ft)	Elevation (m)
Kahaluʻu Ridge	D10	6	3/17–7/18	619,516	2,371,546	21.44236	− 157.84660	328	100
Ka ʻena Point	D11	4	4/17–7/18	577,713	2,383,945	21.55667	− 158.24940	36	11
Kunia III Wells	D12	2	10/17–3/18	601,295	2,366,681	21.39953	− 158.02280	322	98
Lyon Arboretum	D13	5	4/17–7/18	624,183	2,359,481	21.33306	− 157.80250	500	152
Mokuleia F.R	D14	5	4/17–7/18	585,481	2,383,615	21.55333	− 158.17440	548	167
Mokuleia F.R. 2	D15	2	1/18–7/18	583,448	2,382,783	21.54591	− 158.19410	2001	610
Nanakuli F.R	D16	1	4/17–6/17	589,090	2,365,463	21.38917	− 158.14060	167	51
Wahiawa B.G	D17	5	4/17–7/18	602,113	2,378,146	21.50306	− 158.01420	1010	308
Waiāhole F.R	D18	6	3/17–7/18	616,351	2,375,013	21.47389	− 157.87690	623	190
Waianae Kai	D19	4	4/17–3/18	587,481	2,375,570	21.48056	− 158.15560	860	262
Waimea Valley	D20	5	4/17–7/18	597,896	2,392,848	21.63611	− 158.05400	13	4

various processes that can change concentrations is not spatially or temporally uniform. Our aim in analyzing precipitation chemistry is, therefore, to identify which sources and processes are the most significant and to understand how they are distributed within the study area.

Methods

Study area

This study focuses on the Pearl Harbor aquifer on the Island of Oʻahu, Hawaiʻi, USA, the most populous, and third largest island of the Hawaiian Archipelago (Fig. 1). Oʻahu lies between 21° and 22°N and 157° and 159°W. The island is composed of two extinct shield volcanoes, Waiʻanae and the younger Koʻolau (Sherrod et al., 2021). The physiography of Oʻahu is severe and highly variable, characterized by thick rainforests, dramatic elevation gradients, broad, flat, semi-arid regions, and highly urbanized areas, all contained within a 1600-km^2 area (Sherrod et al., 2021).

The climate of Oʻahu is diverse: Mean annual rainfall can vary from 500 to 6500 mm/year over fewer than 30 km (Giambelluca et al., 2013). There are two distinct seasons: a wet season, from November to April, and a dry season, from May to October. The Hawaiian Islands sit in the path of the northeast trade winds, which are a circulation pattern associated with the North Pacific High (Giambelluca, 1983). The trade winds persist more than 90% of the time during summer and approximately 50% during winter, leading to orographic precipitation at high elevations and windward areas (Noguchi, 1979). A variety of weather patterns regulate the wet season climate, including cold fronts, upper-level lows, Kona lows, and subtropical storms (Longman et al., 2021). Although sporadic, these events can often individually supply more than half the annual rainfall in the drier areas of Oʻahu (Dores et al., 2020; Giambelluca, 1983).

Twenty precipitation collectors were deployed throughout the study region to assess rainfall chemistry. Collectors were grouped into several zones, consisting of two to four collectors each. Sampling occurred approximately quarterly. Three collector groups were aimed at assessing elevation transects in key areas of the island. The first elevation transect was deployed along the Manana Ridge trail within the ʻEwa Forest Reserve. It consisted of four collectors distributed between the trailhead (MT1) at 291 m above mean sea level (amsl) and progressing up to the trail summit (MTS) at 806 m amsl. The second elevation transect was deployed along

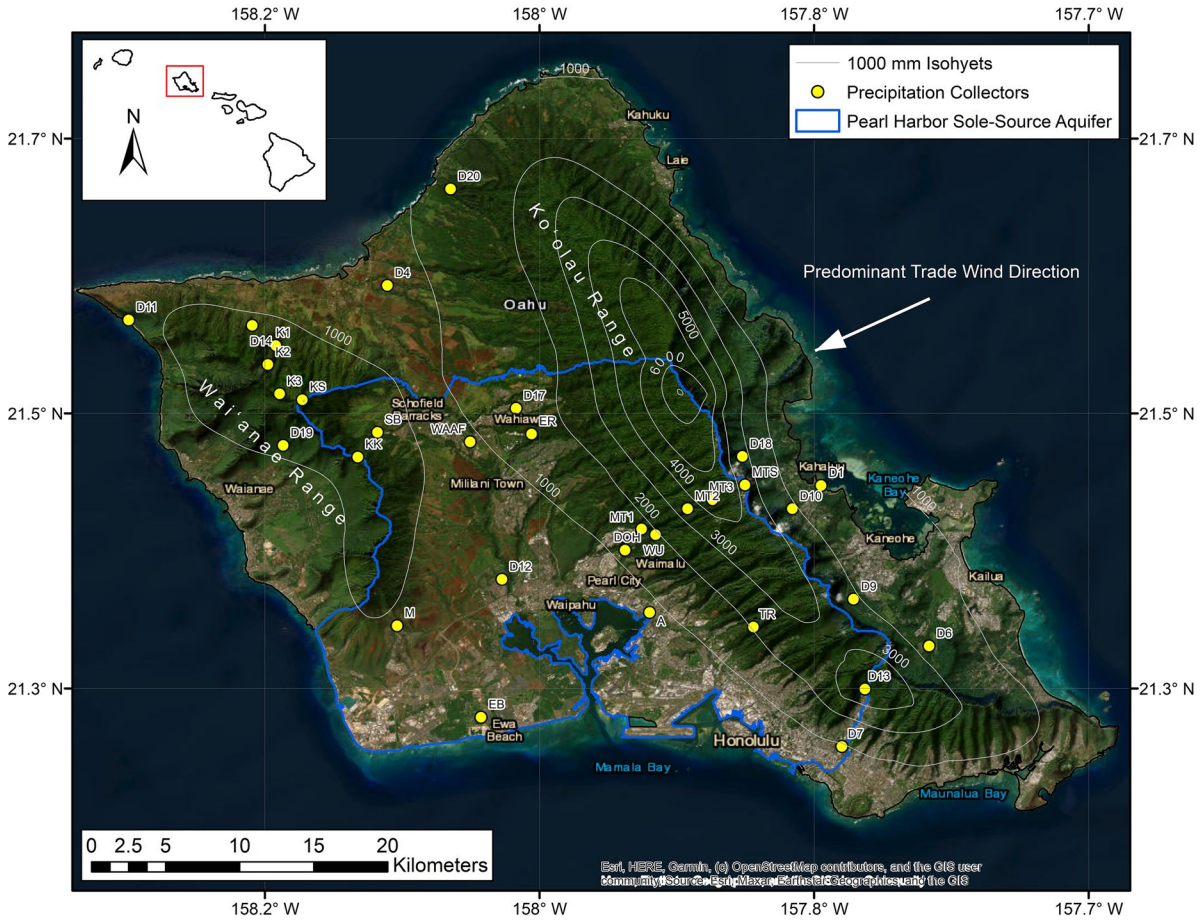

Fig. 1 Map of the study area showing the locations of precipitation collectors and long-term average 1000 mm rainfall contours (isohyets). Collectors from Dores et al. (2020) are included and shown by the designation "D"

Mount Ka'ala Road and included four collectors progressing from 290 m amsl (K1) up to the highest point on O'ahu at 1212 m amsl (KS). The third transect was deployed along the Schofield Plateau, with four collectors distributed generally east-to-west connecting the Wai'anae Range at Kolokole Pass (KK) to the foot of the Ko'olau Range at the East Range Military Training Area (ER). Two collectors were deployed in southwest O'ahu at Makakilo (M) and Ewa Beach (EB). Six collectors were deployed across southcentral O'ahu: Aiea (A), Department of Health (DOH), Tripler Ridge Trail (TR), upper Waimanu Trail (WU), Pu'u Wai'awa (PW), and Mililani High School (MHS). Two collectors were only sampled once due to access constraints related to the COVID-19 pandemic (PW and MHS).

Precipitation collection

The precipitation collectors that were used for this study allowed us to assess bulk rainfall chemistry, which includes both wet and dry deposition. Most precipitation collectors were of the design used in previous studies (Fackrell et al., 2020; Scholl & Ingebritsen, 1995; Scholl et al., 2002; Dores et al., 2020; Booth et al., 2021; Tachera et al., 2021). These collectors consisted of a 5-gal HPDE bucket with a 76- or 110-mm Buchner funnel affixed to the lid. Collectors had an O-ring-sealed spigot installed on the bottom for sample collection. The precipitation collectors were installed in the field on a base with three or four metal support legs for stabilization and ground clearance. A 2-cm-thick layer of high-purity mineral oil in each collector prevented the evaporation of the collected

precipitation. Collectors were covered with black polyethylene bags to reduce biologic productivity in the collectors, which could impact ion compositions. This method also protects against ultraviolet light damage to the plastic buckets. Samples were collected in a triple-deionized-rinsed 500-mL or 60-mL HPDE bottle. The sample bottles were filled completely, forming a convex meniscus at the container mouth to minimize air bubbles, and were refrigerated within six hours of collection to minimize chemical reactions.

Chemical analysis

Preparation for chemical analyses involved collecting an aliquot of each sample from the HPDE field bottles using a syringe. Each sample aliquot was passed through a 0.45-µm filter into a 40-mL vial with a septum or similar container. The vials were filled to the shoulder and then sealed with thin plastic film to minimize evaporation and atmospheric interactions. Samples were analyzed for concentration of major inorganic ions by the Water Resources Research Center laboratory at the University of Hawai'i at Mānoa. Some samples were analyzed for pH and conductivity, but the analysis of this sample subset is not included here. Major inorganic ions were determined using dual Dionex ICS-1100 Ion Chromatographs operated at ambient temperature following the US EPA Method 300.1 (Hautman & Munch, 1997). Anions were separated on a Dionex IonPac AS14A column with 9 mM NA_2CO_3 and 1 mM $NAHCO_3$ eluent. Cations were separated on a Dionex IonPacCS12A column with 20 mM CH_3SO_3H eluent. The flow rate was 1.0 mL/min, with detection by suppressed conductivity. Duplicate sampling was conducted as part of routine lab procedures and indicates relative standard deviations of ± 0.06 mg L^{-1} (F^-), ± 0.26 mg L^{-1} (Cl^-), ± 0.28 mg L^{-1} (Br^-), ± 0.28 mg L^{-1} (SO_4^{2-}), ± 0.06 mg L^{-1} (Na^+), ± 0.15 mg L^{-1} (K^+), ± 0.08 mg L^{-1} (Mg^{2+}), and ± 0.14 mg L^{-1} (Ca^{2+}). Sample precision from the results of similar previous research completed using the same facility and equipment indicate variances among duplicate sample pairs of ± 0.03 mg L^{-1} (F-), ± 1.01 mg L^{-1} (Cl^-), ± 0.03 mg L^{-1} (Br^-), ± 1.82 mg L^{-1} (SO_4^{2-}), ± 0.57 mg L^{-1} (Na^+), ± 0.05 mg L^{-1} (K^+), ± 0.32 mg L^{-1} (Mg^{2+}), and ± 0.66 mg L^{-1} (Ca^{2+}) (Tachera et al., 2021). Field blanks were analyzed to assess sample contamination during sampling procedures and from the practice of recycling of mineral oil. The analysis of the variance between field blanks and reference deionized water indicates the potential contamination of up to 0.04 mg L^{-1} (Cl^-), 0.03 mg L^{-1} (Na^+), 0.01 mg L^{-1} (K^+), 0.01 mg L^{-1} (Mg^{2+}), and 0.07 mg L^{-1} (Ca^{2+}), which, at maximum, constituted less than 3% of the mean sample concentration for each species.

Weather trend analysis

Seasonal precipitation trends were differentiated by analyzing weather data from the International Global Radiosonde Archive (IGRA; Durre et al., 2006, 2016) and observations from monthly weather summaries provided by the National Oceanic and Atmospheric Administration (NOAA/NWS, 2023). The IGRA contains meteorological measurements from daily weather balloon launches at Līhue, on the Island of Kauai. These include elevation profiles of wind direction and speed for each launch. The IGRA data were sifted by selecting measurements below 2500 m amsl, which is generally considered to be the maximum height of the trade wind regime over Hawai'i (Cao et al., 2007). Days when the average wind direction below 2500 m amsl was between 22 and 112° from North were categorized as trade wind days. These assignments were compared with observations in the monthly NOAA summaries. The NOAA summaries were also used to identify periods when cold fronts, Kona lows, upper-level lows, and tropical cyclones delivered rainfall to O'ahu. The results from this analysis were overlaid on the precipitation chemistry data utilizing "rug" plots (Wickam et al., 2016).

Data analysis

The overarching goal of our data analyses was to identify the contributions of terrestrial, marine SSA, and anthropogenic inputs to the bulk precipitation chemistry within and around the Pearl Harbor aquifer and to observe how they vary in time and space. A review of relevant precipitation chemistry studies highlighted several methods which guided the analyses of the data presented herein. We computed a rainfall volume-weighted average (VWA) chemistry for each collector location and major ion to highlight the long-term

spatial trends in the inorganic ion deposition (Akpo et al., 2015; Keresztesi et al., 2020; Lee et al., 2000; Lu et al., 2011; Scholl & Ingebritsen, 1995). We calculated total and wet deposition to give a sense of the differing masses of chemical constituents entering the nutrient cycle in each sampling interval (Akpo et al., 2015; Lee et al., 2000). Wet deposition was calculated by multiplying the VWA ion concentration by long-term average annual precipitation (Frazier & Giambelluca, 2017). Total deposition was measured by multiplying each sample concentration by the measured precipitation and summing these values over a year. We used correlation analysis to quantify the relationships among different ions and to assess the impacts of various environmental and meteorological factors on precipitation chemistry (Akpo et al., 2015; Keene et al., 1986; Keresztesi et al., 2020; Kroopnick, 1977; Li et al., 2007; Lu et al., 2011). We conducted principal component analysis (PCA) to parse out different sources of precipitation inorganic constituents (Keresztesi et al., 2020; Lee et al., 2000; Li et al., 2007; Shi et al., 2009). To assess crustal and anthropogenic inorganic sources more closely, we completed a SSA correction, which is a procedure that differentiates chemical contributions from marine SSAs by correcting bulk chemistry based on a reference species (Akpo et al., 2015; Keene et al., 1986; Lee et al., 2000; Lu et al., 2011; Saltzman et al., 1986; Satake & Yamane, 1992; Scholl & Ingebritsen, 1995). Finally, we completed spatial interpolations via ordinary kriging and inverse distance weighting (power two) to aid in visualizing spatial variations of nutrient deposition (Keresztesi et al., 2020; Pearson & Fisher, 1971; Scholl & Ingebritsen, 1995). Several calculations warrant a more detailed explanation, as described in the sections below.

Sea salt aerosol correction

The non-sea salt (NSS) fraction of each chemical species in precipitation was calculated by completing SSA corrections. This procedure removed the estimated SSA fraction of each species from bulk precipitation. The SSA fraction of a chemical species was calculated by selecting a reference species and multiplying the concentration of the reference species in the sample by the seawater ratio of that chemical species to the reference species, such that

$$C_{ssa} = \frac{C_{sw}}{R_{sw}} \cdot R_s \tag{1}$$

where C_{ssa} is the sea salt fraction of each chemical species C, C_{sw}/R_{sw} is the seawater ratio of each chemical species C to the reference species R, and R_s is the concentration of the reference species in the sample. The NSS fraction of the chemical species C_{nss} was calculated by subtracting the SSA fraction from the total concentration of that species,

$$C_{nss} = C_s - C_{ssa} \tag{2}$$

where C_S is the concentration of each chemical species C in the sample. The accuracy of this procedure depends on two assumptions: to begin with, the reference species must be sourced solely from SSAs; additionally, there should not be significant fractionation of that species relative to the other sea salt constituents during mobilization, transport, and deposition (Keene et al., 1986).

Crustal and marine enrichment factors

Crustal and marine enrichment factors (*EF*) were calculated to compare precipitation chemistry with the average compositions of seawater (Keene et al., 1986; Pilson, 1998; Wilson, 1975) and continental crust (Kring, 1997) according to the expressions

$$EF_{sw} = \frac{\frac{C_s}{R_s}}{\frac{C_{sw}}{R_{sw}}} \tag{3}$$

$$EF_{cr} = \frac{\frac{C_s}{R_s}}{\frac{C_{cr}}{R_{cr}}} \tag{4}$$

where C_S is the concentration of species C in the sample, R_S is the concentration of the reference species R in the sample, C_{SW}/R_{SW} is the average ratio of species C to reference species R in seawater, and C_{CR}/R_{CR} is the average ratio of species C to reference species R in the continental crust. The accuracy of marine and crustal EFs depends on the same assumptions as SSA corrections.

Regression analysis

Regression analysis was used to determine the SSA origin for inorganic ions in precipitation (Akpo et al.,

2015; Keene et al., 1986; Khemani et al., 1985). This procedure is based on the observation that, though the composition of ocean water varies across the globe, the relative ratios of inorganic ions in seawater are consistent (Keene et al., 1986; Lewis & Schwartz, 2004; Table 3). If the regression coefficients of meteoric chemical ratios were not significantly different from those of seawater (within the 95% confidence intervals), we assessed that both species originated primarily from SSAs (Keene et al., 1986). Regression analysis was also used to parse bulk deposition into dry and wet deposition following Pearson and Fisher (1971). Following this work, wet deposition was assessed to be the most probable deposition mode if regression analysis of rainfall rates (mm day^{-1}) vs. bulk deposition (g ha^{-1} day^{-1}) produced $p \leq 0.05$, r-squared ≥ 0.5, and a positive slope. When these conditions were not met, dry deposition, or a combination of both dry and wet depositions, was assumed to be the dominant deposition mode.

Principal component analysis

PCA is a common statistical technique that can be used to simplify multivariate datasets (Abdi & Williams, 2010). The goal of PCA is to reduce the dimensionality of a dataset by analyzing the structure of the data and the interrelationships among variables. The principal components are displayed in a loading matrix. Each column in the loading matrix contains the eigenvector of each variable for a particular principal component. The total eigenvalue for that component is usually added as an additional row at the bottom of the loading matrix. The eigenvectors communicate the weight or loading each variable gives within that principal component. The eigenvalue, often called inertia, reflects the importance of that principal component in the overall dataset. The inertia of each component is usually displayed as a percentage of the total inertia of the dataset (the sum of all eigenvalues). The inertia of a component communicates the amount of variance within the dataset that is explained by that component. The principal components can be viewed as the primary sources of variability within the dataset. In studies of bulk precipitation chemistry, principal components are interpreted to be the principal sources of chemical constituents (Keresztesi, et al., 2020; Lee et al., 2000; Li et al., 2007; Shi et al., 2009).

Results and discussion

The following consists of four sections grouped by major ions which contain results and discussion subsections.

Sodium and chloride

Results

Sodium and Cl^- were the most abundant constituents in bulk precipitation, exceeding other ions by an order of magnitude in most samples. Volume-weighted average concentrations ranged from 4.5 ± 1.0 mg L^{-1} Cl^- and 3.2 ± 0.8 mg L^{-1} Na^+ at Ka'ala Summit to 39.7 ± 2.3 mg L^{-1} Cl^- and 22.9 ± 1.8 mg L^{-1} Na^+ at Ka'ena Point (Table 2; Fig. 2). The highest sample concentrations of Na^+ and Cl^-, excluding samples taken from the Ka'ena Point collector (D11), were detected between May 10, 2019, and July 11, 2019, along the Manana Ridge transect at the two lowest-elevation collectors (290 m and 450 m amsl). Sample concentrations were 60.8 mg L^{-1} Cl^- and 40.8 mg L^{-1} Cl^- at MT1 and MT2, respectively. Sample contamination was ruled out due to proportional enrichment in those samples of both SO_4^{2-} and Mg^{2+} consistent with marine sea salt origin and similar enrichment at other collectors in the vicinity.

Concentrations of Na^+ and Cl^- were strongly correlated, indicating a predominantly marine SSA origin for these species. Reduced major axis (RMA) regression analysis of precipitation Na^+ vs. Cl^- produced a slope of 0.878 ± 0.35, an intercept of 10.101 ± 11.31, a Spearman correlation coefficient of 0.99, and $p < 0.01$ (Table 3). The results of the RMA regression are consistent with SSA origin (Keene et al., 1986). The principal component analysis further corroborates SSA origin for meteoric Na^+ and Cl^-. The PCA loading matrix shows that approximately 90% of the variability in the major ions in precipitation is related to a parameter weighted heavily by Na^+ and Cl^- concentrations (Table 4; Abdi & Williams, 2010).

Discussion

Another important control on Na^+ deposition may be related to atmospheric dust: many of our samples showed an apparent excess of Na^+ relative to the seawater molar sodium-chloride ratio of 0.86. Long-range atmospheric

Table 2 Precipitation volume-weighted average chemistry and uncertainty calculated from samples collected on O'ahu, HI, USA, between Mach 2017 and June 2021

		Precipitation volume-weighted average concentration (mg L^{-1})											
Location description	Abbreviation	Cl^-	ΔCl^-	Na^+	ΔNa^+	Ca^{2+}	ΔCa^{2+}	K^+	ΔK^+	SO_4^{2-}	ΔSO_4^{2-}	Mg^{2+}	ΔMg^{2+}
Kaala Gate 3	K1	6.69	1.10	4.44	0.85	0.70	0.82	0.50	0.28	0.86	1.34	0.49	0.57
Kaala Milepost 3	K2	4.70	1.07	3.25	0.83	2.36	0.87	0.38	0.28	0.56	1.19	0.34	0.57
Kaala Culvert 49	K3	4.77	1.06	3.37	0.82	0.90	0.82	0.69	0.30	0.35	0.91	0.39	0.57
Kaala Summit	KS	4.48	1.03	3.16	0.79	0.50	0.81	0.27	0.25	0.60	1.26	0.32	0.57
Manana Trailhead	MT1	11.31	1.17	6.87	0.89	2.30	0.83	0.42	0.24	1.82	1.33	1.01	0.58
Manana Trail 2	MT2	12.34	1.18	7.46	0.90	1.03	0.82	0.36	0.25	1.80	1.30	0.93	0.58
Manana Trail 3	MT3	6.87	1.04	4.50	0.79	1.31	0.82	0.24	0.24	0.96	1.35	0.54	0.57
Manana Trail Summit	MTS	7.63	1.13	5.09	0.88	1.34	0.83	0.45	0.27	0.86	1.35	0.44	0.57
Ewa Beach	EB	5.50	1.21	3.53	0.93	5.08	1.13	0.26	0.27	0.93	1.29	0.50	0.58
Tripler Ridge	TR	10.25	1.18	6.33	0.91	1.25	0.82	0.40	0.26	1.46	1.30	0.63	0.57
Makakilo	M	7.85	1.24	5.09	0.97	2.27	0.90	0.36	0.28	1.85	1.36	0.57	0.58
Kolekole Pass	KK	7.02	1.15	3.40	0.84	3.98	0.91	1.06	0.39	0.88	1.25	0.94	0.58
Schofield Barracks	SB	6.26	1.29	4.04	1.00	2.64	0.97	0.84	0.44	0.77	1.06	0.57	0.59
Wheeler Army Airfield	WAAF	11.18	1.31	6.01	0.96	2.34	0.85	2.59	0.62	1.59	1.32	1.16	0.59
East Range	ER	10.53	1.30	5.99	0.98	2.43	0.86	0.51	0.31	1.23	1.35	0.68	0.58
Aiea	A	11.55	1.60	6.55	1.21	0.91	0.84	0.36	0.31	2.12	1.37	0.77	0.61
Dept. of Health	DOH	14.90	1.57	8.53	1.19	0.75	0.84	1.24	0.47	2.56	1.34	0.87	0.60
Waimanu Upper	WU	9.55	1.28	5.36	0.96	0.32	0.81	0.28	0.26	1.66	1.35	0.58	0.58
Kamehameha Hwy	D1	12.87	1.35	6.98	1.01	1.02	0.82	0.80	0.33	2.45	1.36	0.80	0.58
Haleiwa Wells	D4	16.70	1.96	9.59	1.49	3.42	0.98	4.86	1.01	2.11	1.39	1.62	0.69
Hawai 'i Ag. Center	D6	9.84	1.13	6.18	0.87	3.19	0.85	0.34	0.21	1.93	1.35	0.93	0.57
HIG UH Mānoa	D7	15.89	1.58	10.19	1.25	5.19	1.08	0.44	0.27	3.20	1.37	1.32	0.61
Ho'omaluhia B.G	D9	7.17	1.08	4.92	0.84	4.27	0.87	0.24	0.18	1.36	1.23	0.83	0.57
Kahalu'u Ridge	D10	7.47	1.07	4.73	0.82	2.72	0.84	0.30	0.21	1.49	1.35	0.92	0.57
Ka 'ena Point	D11	39.70	2.33	22.93	1.77	5.65	1.03	1.37	0.43	7.02	1.45	2.96	0.73
Kunia III Wells	D12	10.10	1.63	5.55	1.21	4.07	1.09	5.47	1.15	3.16	1.41	1.30	0.67
Lyon Arboretum	D13	10.37	1.09	6.17	0.83	3.26	0.83	0.22	0.18	2.16	1.35	1.19	0.57
Mokuleia F.R	D14	8.00	1.22	5.23	0.96	3.36	0.90	0.82	0.35	1.69	1.35	1.06	0.60
Wahiawa B.G	D17	12.79	1.34	8.06	1.05	5.73	0.98	1.35	0.40	1.81	1.20	1.42	0.60
Waiāhole F.R	D18	10.23	1.12	6.48	0.87	4.37	0.85	0.31	0.20	1.64	1.35	0.95	0.57
Waianae Kai	D19	10.24	1.33	6.13	1.02	5.73	1.03	1.39	0.45	2.53	1.36	1.07	0.60
Waimea Valley	D20	10.80	1.20	6.66	0.92	7.82	1.01	0.64	0.25	1.58	1.35	1.31	0.59

dust transport is a reasonable explanation for this excess Na^+, suggesting Cl^- is a more appropriate reference species to use in sea salt corrections. However, due to the possibility of Cl^- depletion from SSAs through reaction with weak organic and inorganic acids (Laskin et al., 2012), it was not possible to differentiate the apparent enrichment in Na^+ from the depletion of Cl^- without comparing Na^+ and Cl^- concentrations to other major SSA constituents. Sulfate and Mg^{2+} were therefore plotted against Cl^- and Na^+ to assess whether the apparent Na^+ excess was due to depletion of Cl^- or a true NSS Na^+ source. Chloride fractionation would manifest as a regression slope greater than the magnesium- and sulfate-to-chloride seawater ratio slopes when compared to the magnesium- and sulfate-to-sodium seawater ratio slopes. Sodium enrichment from an atmospheric source would manifest as a regression slope generally parallel to the seawater ratio slopes but with a negative *y*-intercept. Results from this analysis (Fig. 4) indicate Cl^- depletion was negligible. The reduced major axis regression slopes

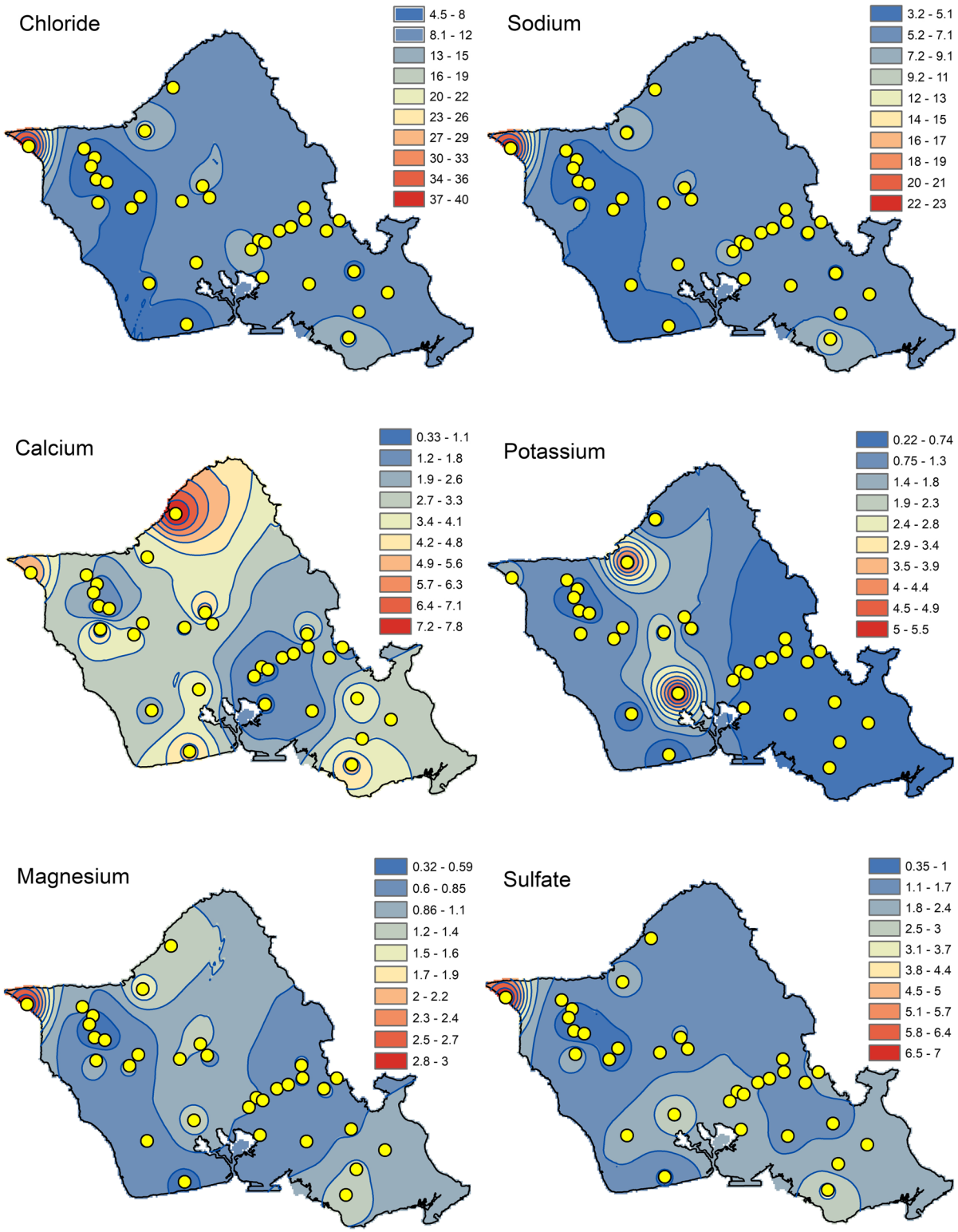
Chloride
4.5 - 8
8.1 - 12
13 - 15
16 - 19
20 - 22
23 - 26
27 - 29
30 - 33
34 - 36
37 - 40
Sodium
3.2 - 5.1
5.2 - 7.1
7.2 - 9.1
9.2 - 11
12 - 13
14 - 15
16 - 17
18 - 19
20 - 21
22 - 23
Calcium
0.33 - 1.1
1.2 - 1.8
1.9 - 2.6
2.7 - 3.3
3.4 - 4.1
4.2 - 4.8
4.9 - 5.6
5.7 - 6.3
6.4 - 7.1
7.2 - 7.8
Potassium
0.22 - 0.74
0.75 - 1.3
1.4 - 1.8
1.9 - 2.3
2.4 - 2.8
2.9 - 3.4
3.5 - 3.9
4 - 4.4
4.5 - 4.9
5 - 5.5
Magnesium
0.32 - 0.59
0.6 - 0.85
0.86 - 1.1
1.2 - 1.4
1.5 - 1.6
1.7 - 1.9
2 - 2.2
2.3 - 2.4
2.5 - 2.7
2.8 - 3
Sulfate
0.35 - 1
1.1 - 1.7
1.8 - 2.4
2.5 - 3
3.1 - 3.7
3.8 - 4.4
4.5 - 5
5.1 - 5.7
5.8 - 6.4
6.5 - 7

◂**Fig. 2** Interpolated precipitation volume-weighted average chemistry of six major ions on the island of O'ahu, HI, USA. Interpolation method was inverse distance weighted, power two. Coverages were interpolated from the precipitation collector locations represented by yellow circles. Data from Dores et al. (2020) is included. Units are in milligrams per liter

on Fig. 4 B and C (Mg^{2+} vs. Cl^- and Mg^{2+} vs. Na^+) vary indistinguishably from the seawater ratios, as do those on Fig. 4 D and E (SO_4^{2-} vs. Cl^- and SO_4^{2-} vs. Na^+). Samples with excess Na^+ also plotted more consistently below the seawater ratio slopes which suggests a NSS Na^+ source, though uncertainties were too great to definitively say either species produced a negative y-intercept (Table 3). Chloride was therefore selected as the reference species for the SSA correction.

Sea salt aerosol correction results corroborate a non-marine source of Na^+. The propagated error for NSS Na^+ was ± 0.80 mg L^{-1}. This uncertainty was large due to the compounding effect of instrumental uncertainty for both Cl^- (± 1.01 mg L^{-1}) and Na^+ (± 0.66 mg L^{-1}). Even with the higher uncertainty, there was a strong trend in NSS Na^+ across most collectors throughout the dataset. Excluding samples from two collectors where there were overcorrections producing negative NSS Na^+ values (WAAF and KK), NSS Na^+ concentrations for all collectors and all samples were within a narrow range of 1.15 mg L^{-1}. This uniformity is striking and necessitates a NSS Na^+ source that is evenly distributed across the entire sample area, with atmospheric dust being a more plausible mechanism than local dust transport, which would be expected to be more spatially variable. Analysis of wind patterns from International Global Radiosonde Archive (IGRA) data taken at Līhue (Durre et al., 2006, 2016), and monthly weather summaries provided by the National Oceanic and Atmospheric Administration (NOAA/NWS, 2023), shows an inverse relationship between trade winds and NSS Na^+ deposition (Fig. 3). During dry seasons, when trade winds were more consistent, NSS Na^+ deposition was low. During wet seasons, when the trades were inconsistent and disturbance-based weather events were more frequent, NSS Na^+ was consistently elevated. These elevated NSS Na^+ deposition periods coincided with seasonal shifts in atmospheric wind source trajectories to more remote, north-northwesterly locations and higher altitudes (Torri et al., 2023), suggesting Asian continental dust as a likely source of NSS Na^+ (Fig. 4).

Calcium

Results

Calcium was the third most abundant constituent in bulk precipitation, below chloride and sodium. Volume-weighted average Ca^{2+} and propagated uncertainty ranged from 0.32 ± 0.81 mg L^{-1} Ca^{2+} at Waimano Trail (WU) to 7.82 ± 1.00 mg L^{-1} Ca^{-2+} at Waimea Valley (D20) (Table 2). Individual sample uncertainty based on duplicates was 0.66 mg L^{-1} Ca^{2+} (Tachera et al., 2021). The highest single sample concentration was 39.74 mg L^{-1} collected at Ewa Beach between June 23, 2020, and October 16, 2020. Results from the SSA correction indicate most precipitation Ca^{2+} was non-marine; the propagated NSS uncertainty was low at ± 0.66 mg L^{-1} NSS Ca^{2+}.

Discussion

Bulk precipitation chemistry data suggest at least one NSS Ca^{2+} source. Calcium in precipitation is often attributed to crustal dust transport (Brahney et al., 2013; Loye-Pilot et al., 1986; Niu et al., 2014; Szép et al., 2018; Xiao, 2016; Zhang et al., 2003). Long-range transport is possible; however, a more spatially uniform distribution of NSS Ca^{2+} would be expected across all precipitation collectors, as was observed with NSS Na^+. This trend was not apparent in Ca^{2+} concentrations, which were generally higher in coastal areas and lower at high elevations (Fig. 2). Regression analysis of rainfall rates (mm day^{-1}) vs. Ca^{2+} bulk deposition (g ha^{-1} day^{-1}) suggests that Ca^{2+} is delivered primarily through dry deposition, though there were no obvious correlations to weather or location (Table 5).

There are two probable local sources of NSS Ca^{2+}. The first is O'ahu's coastal alluvial deposits, mainly composed of calcite-cemented shallow marine sediments (Fletcher et al., 2008; Sherrod et al., 2021). Volume-weighted average Ca^{2+} exceeded 5 mg L^{-1} at five locations that resided on or close to such deposits: Ka'ena Point (D11), the University of Hawai'i at Mānoa (UHM) campus (D7), Wai'anae Kai (D19), Waimea Valley (D20), and Ewa Beach (EB) (Fig. 5). Marine enrichment factors of Ca^{2+} were also elevated near these deposits (Fig. 5). The Ewa Beach collector is notable in that it also resided within a high-growth suburban area where there was extensive vegetation

Table 3 Regression analysis of seawater (SW) and bulk precipitation major ion molar ratios. A reduced major axis (RMA) regression was used due to uncertainty in both variables. Ninety-five percent confidence intervals (CI) were calculated to assess agreement with the seawater ratios. Seawater molar ratios were taken from Pilson (1998). Shaded cells identify regression slopes and intercepts that fall within the 95% CI for the SW molar ratios, indicating predominantly sea salt aerosol origin. P-values for all regressions were less than 0.01

Ions	Seawater Ratios	RMA Slope	RMA Intercept	Correlation Coefficient
Na/Cl	0.859	0.878 ± 0.35	10.101 ± 11.31	0.99
Mg/Cl	0.097	0.108 ± 0.01	2.595 ± 3.67	0.90
SO_4/Cl	0.052	0.076 ± 0.01	-4.473 ± 3.64	0.79
Ca/Cl	0.019	0.331 ± 0.08	-40.955 ± 25.38	0.19
K/Cl	0.019	0.237 ± 0.04	-49.976 ± 11.31	0.29
Mg/Na	0.113	0.123 ± 0.01	1.351 ± 3.93	0.89
SO_4/Na	0.060	0.086 ± 0.01	-5.345 ± 3.59	0.81
Ca/Na	0.022	0.377 ± 0.09	-44.764 ± 26.34	0.18
K/Na	0.022	0.270 ± 0.06	-52.703 ± 18.62	0.24
SO_4/Mg	0.534	0.700 ± 0.10	-6.289 ± 3.85	0.79
Ca/Mg	0.195	3.061 ± 0.69	-48.899 ± 25.68	0.38
K/Mg	0.193	2.192 ± 0.50	-55.663 ± 18.46	0.37

stripping and excavation during the study period. Such activity has been connected with increased mineral dust transport elsewhere (Brahney et al., 2013; Neff et al., 2005). The other probable source for NSS Ca^{2+} is cement production operations, which also tend to be concentrated in O'ahu's southern coastal plains. Dominant wind direction links these potential calcite sources with areas showing elevated NSS Ca^{2+} deposition. Weather data show that Ca^{2+} deposition generally increased during periods of persistent trade winds (Fig. 6). The principal component analysis also implicates calcium-rich dust transport. Principal component 2 accounted for approximately 6% of the variability in the major ions and was strongly weighted by Ca^{2+} concentrations (Table 4; Abdi & Williams, 2010). These spatiotemporal trends indicate that mineral dust transport from local alluvial deposits and cement production activity are the two most probable NSS sources for Ca^{2+} in bulk precipitation chemistry.

Potassium

Results

Potassium concentrations in samples were generally low, constituting less than 3% of the measured ion load on average. Volume-weighted average K^+ ranged from 0.22 ± 0.18 mg L^{-1} K^+ at Lyon Arboretum

Table 4 Rotation matrix displaying the results from principal component analysis completed on bulk precipitation chemistry. The principal components (PC) can be viewed as the primary sources of variability within the dataset. In studies of bulk precipitation chemistry, the principal components are interpreted to be the principal sources of chemical constituents (Keresztesi et al., 2020; Lee et al., 2000; Li et al., 2007; Shi et al., 2009)

	PC1	PC2	PC3	PC4	PC5	PC6
Chloride	−0.75	−0.03	0.09	0.65	−0.04	−0.07
Sulfate	−0.05	0.01	0.01	−0.16	−0.81	−0.56
Sodium	−0.65	−0.06	−0.17	−0.72	0.15	0.03
Potassium	−0.05	0.15	0.97	−0.18	0.07	−0.02
Magnesium	−0.07	0.07	0.04	−0.03	−0.56	0.82
Calcium	−0.05	0.98	−0.16	0.00	0.05	−0.05
% of total variance explained	91.14	5.50	2.65	0.53	0.11	0.06

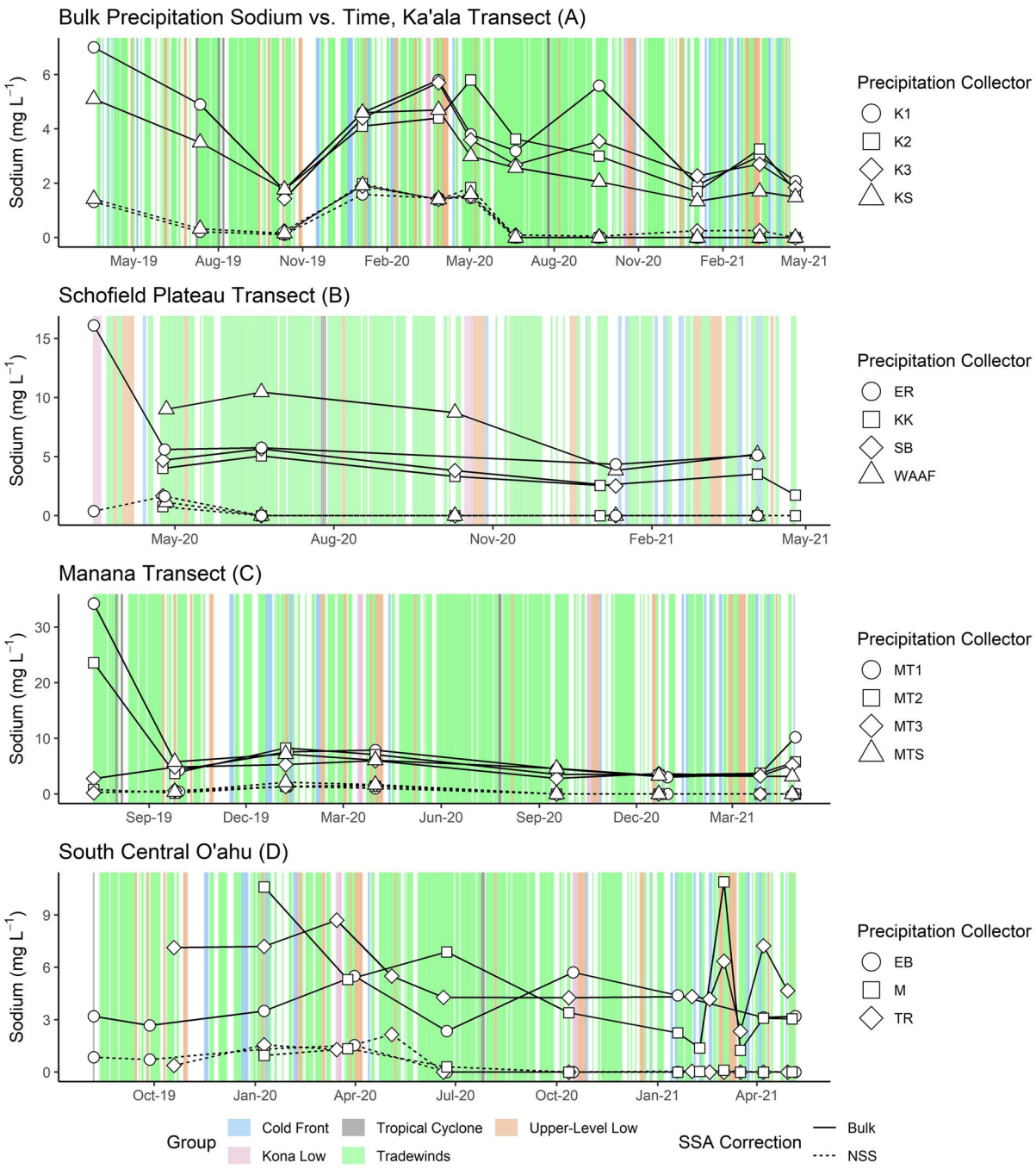

Fig. 3 Time series of bulk precipitation Na^+ concentrations taken on O'ahu, HI, USA. Ka'ala Transect (**A**), Schofield Plateau Transect (**B**), Manana Transect (**C**), and Southcentral O'ahu collectors (**D**). Non-sea salt (NSS) contributions are displayed in dotted lines. Non-sea salt uncertainty was ± 0.80 mg L^{-1}. Weather trend data derived from International Global Radiosonde Archive (IGRA) weather balloon launces at Līhue, Kauai (Durre et al., 2006, 2016) and from monthly weather summaries provided by the National Oceanic and Atmospheric Administration (NOAA/NWS, 2023) are shown in the background

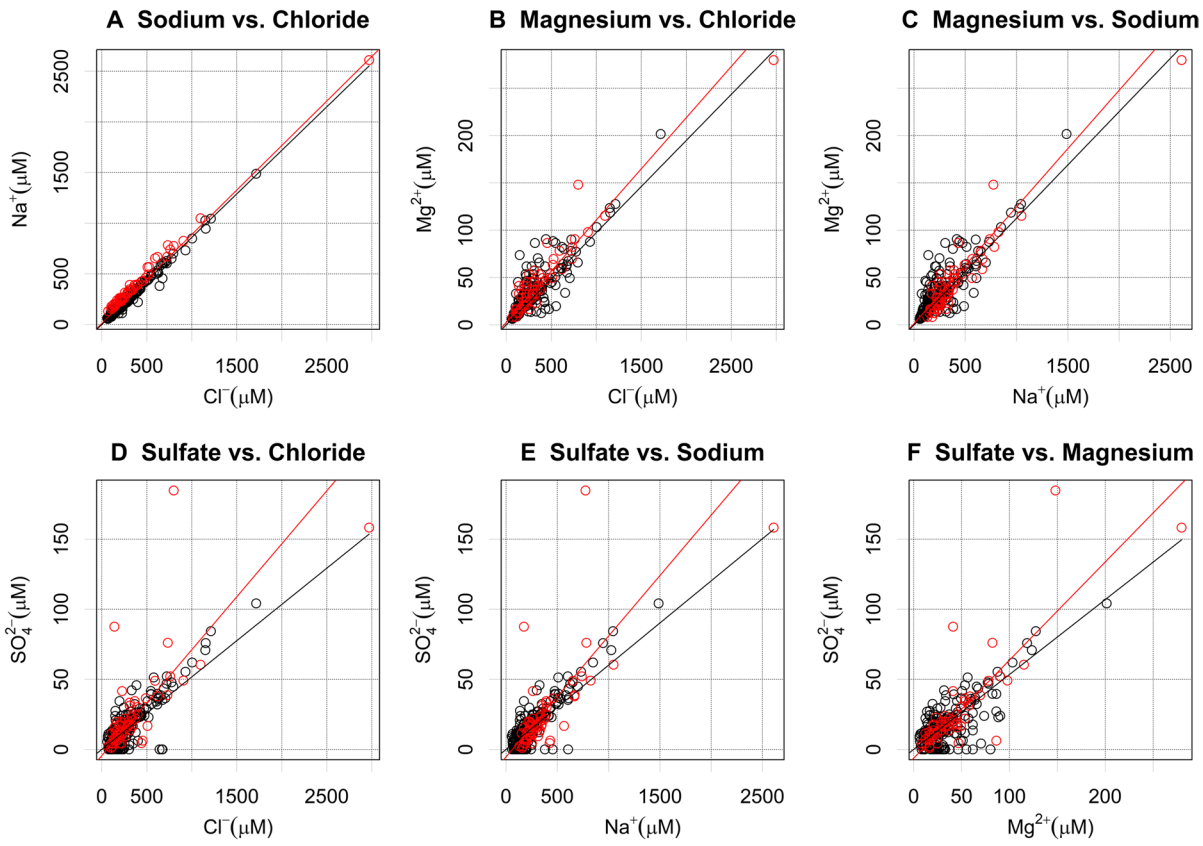

Fig. 4 Plots of major sea salt constituents (Cl^-, Na^+, Mg^{2+}, and SO_4^{2-}) relative to seawater ratios in bulk precipitation from O'ahu, HI, USA. The red line displays reduced major axis regression fits for each plot. The black lines display the seawater ratios for each major ion pair (Pilson, 1998). Red points display samples with > 40 µmol L^{-1} Na^+ excess relative to the chloride:sodium seawater ratio

(D13) to 5.47 ± 1.15 mg L^{-1} K^+ at Kunia III Wells (D12). The ratio of potassium-to-chloride in bulk precipitation exceeded the seawater molar ratio of 0.02 in nearly all samples. Instrumental precision based on duplicate sampling was ± 0.05 mg L^{-1} K^+ (Tachera et al., 2021), which rules out uncertainty as the sole culprit for excess NSS K^+. Sea salt aerosol correction results confirm that NSS sources of K^+ dominated, whereas propagated error through the SSA correction was low (± 0.06 mg L^{-1} NSS K^+).

The data suggest local NSS K^+ sources contribute to bulk precipitation chemistry. There were notable spikes in NSS K^+ at select locations. Concentrations of NSS K^+ exceeded 1.95 mg L^{-1} in one or more samples at Kolekole Pass (KK), Schofield Barracks (SB), Wheeler Army Airfield (WAAF), East Range (ER), Hale'iwa (D4), Ka'ena Point (D11), Kunia (D12), Mokulē'ia (D14), Wahiawa (D17), Wai'anae Kai (D19), and Waimano Ridge (DOH) (Fig. 2). Excluding Ka'ena Point, the proximity of these collectors to populated and/or agricultural areas suggests a possible connection with fertilizer use, which is consistent with findings in other precipitation chemistry studies (Keresztesi et al., 2020; Lu et al., 2011). Interpolated coverages of average annual bulk deposition and crustal and marine enrichment factors show elevated K^+ deposition in central O'ahu, near the island's main agricultural areas (Fig. 7). Regression analysis of rainfall rates (mm day^{-1}) vs. K^+ bulk deposition (g ha^{-1} day^{-1}) indicates that dry deposition is the most likely delivery mode (Table 5).

Table 5 Regression analysis of rainfall rates (mm day−1) vs. bulk deposition (g ha−1 day−1). Cells colored blue are those that met three conditions: $p \leq 0.05$, r-squared ≥ 0.5, and positive slope, indicating wet deposition as the most probable deposition mode. Red colored cells represent collectors where these conditions were not met, and thus, where dry deposition, or a combination of both dry and wet deposition, was assumed to be the dominant deposition modes (Pearson & Fisher, 1971).

	Ion	Chloride				Sodium				Calcium				Sulfate				Magnesium				Potassium			
Collector	n	b	m	r	p	b	m	r	p	b	m	r	p	b	m	r	p	b	m	r	p	b	m	r	p
K1	11	1.00	0.01	0.77	0.00	1.38	0.02	0.70	0.00	1.44	0.09	0.47	0.02	2.25	0.06	0.42	0.03	0.67	0.17	0.84	0.00	0.83	0.17	0.37	0.05
K2	9	0.72	0.02	0.80	0.00	1.00	0.02	0.66	0.01	2.68	0.01	0.37	0.08	2.62	0.07	0.40	0.07	0.67	0.17	0.84	0.00	3.77	0.01	0.00	0.94
K3	9	1.50	0.01	0.76	0.00	1.87	0.02	0.62	0.01	0.95	0.09	0.71	0.00	4.32	0.03	0.08	0.46	1.49	0.18	0.56	0.02	0.69	0.13	0.73	0.00
KS	11	1.97	0.02	0.62	0.00	3.06	0.02	0.45	0.02	0.27	0.19	0.72	0.00	3.63	0.09	0.50	0.02	1.94	0.24	0.62	0.00	6.61	0.01	0.00	0.95
MT1	12	3.58	0.00	0.32	0.05	3.40	0.01	0.36	0.04	4.68	0.01	0.08	0.37	4.03	0.02	0.22	0.12	2.98	0.05	0.32	0.06	5.33	0.04	0.09	0.33
MT2	8	7.90	0.00	0.19	0.28	7.73	0.00	0.23	0.23	8.48	0.01	0.04	0.63	8.14	0.01	0.19	0.29	7.86	0.02	0.19	0.28	8.23	0.03	0.13	0.37
MT3	8	3.10	0.01	0.89	0.00	5.14	0.01	0.88	0.00	14.85	-0.01	0.03	0.68	3.71	0.07	0.84	0.00	3.78	0.13	0.53	0.04	9.34	0.10	0.17	0.31
MTS	6	0.92	0.01	0.78	0.02	1.90	0.01	0.67	0.05	4.86	-0.01	0.03	0.72	1.24	0.08	0.92	0.00	1.15	0.16	0.73	0.03	2.24	0.11	0.34	0.22
EB	9	0.04	0.02	0.93	0.00	-0.12	0.03	0.96	0.00	0.31	0.02	0.48	0.04	0.47	0.08	0.86	0.00	0.12	0.21	0.84	0.00	0.59	0.19	0.78	0.00
TR	12	1.68	0.01	0.64	0.00	1.80	0.01	0.59	0.00	7.40	0.01	0.01	0.73	2.39	0.05	0.62	0.00	1.01	0.16	0.63	0.00	0.18	0.29	0.62	0.00
M	10	1.58	0.01	0.38	0.06	1.86	0.01	0.39	0.05	3.25	0.01	0.02	0.70	0.46	0.06	0.60	0.01	1.82	0.12	0.33	0.09	2.09	0.17	0.33	0.08
KK	6	0.46	0.01	0.94	0.00	0.60	0.03	0.93	0.00	0.73	0.02	0.92	0.00	1.96	0.07	0.82	0.01	0.68	0.09	0.97	0.00	-2.29	0.14	0.83	0.01
SB	4	-0.47	0.02	0.99	0.00	0.28	0.02	0.96	0.02	1.38	0.01	0.02	0.87	0.74	0.07	0.84	0.08	-0.84	0.26	0.85	0.08	1.18	0.04	0.05	0.78
WAAF	5	-0.50	0.01	0.97	0.00	-0.33	0.02	0.92	0.01	-0.19	0.05	0.99	0.00	0.40	0.06	0.95	0.01	-0.20	0.09	1.00	0.00	-2.21	0.06	0.33	0.31
ER	5	3.04	0.00	0.31	0.33	2.91	0.01	0.31	0.33	1.21	0.04	0.45	0.21	4.18	0.01	0.12	0.57	2.35	0.07	0.43	0.23	5.23	0.01	0.01	0.87
D6	4	0.84	0.01	0.95	0.03	1.97	0.01	0.62	0.21	30.44	-0.06	0.57	0.24	4.55	0.03	0.42	0.35	3.71	0.07	0.39	0.37	7.42	0.08	0.66	0.19
D7	4	-0.71	0.01	0.80	0.11	0.05	0.01	0.63	0.21	4.59	-0.01	0.25	0.50	0.07	0.03	0.67	0.18	0.05	0.07	0.65	0.19	2.04	0.08	0.86	0.07
D9	4	1.67	0.01	0.91	0.05	3.24	0.01	0.91	0.05	5.69	0.01	0.64	0.20	4.86	0.04	0.77	0.12	3.06	0.08	0.98	0.01	9.71	-0.01	0.01	0.91
D10	5	5.02	0.01	0.68	0.09	5.96	0.01	0.64	0.10	17.03	-0.02	0.26	0.38	4.16	0.04	0.90	0.01	4.89	0.07	0.95	0.00	9.86	0.05	0.26	0.38
D11	4	2.96	0.00	0.04	0.80	3.12	0.00	0.02	0.85	-2.31	0.03	0.18	0.57	1.88	0.01	0.10	0.69	1.52	0.02	0.24	0.51	2.67	0.02	0.22	0.53
D13	4	9.80	0.00	0.59	0.23	8.11	0.01	0.83	0.09	13.39	0.01	0.39	0.38	6.71	0.03	0.92	0.04	7.83	0.05	0.90	0.05	15.77	0.04	0.11	0.67
D14	4	1.64	0.01	0.89	0.05	1.12	0.01	0.99	0.01	-3.32	0.06	0.69	0.17	0.84	0.04	0.97	0.01	0.75	0.07	0.75	0.14	3.31	0.00	0.00	0.99
D17	4	2.88	0.00	0.60	0.23	2.99	0.00	0.70	0.16	4.28	0.00	0.03	0.82	4.26	0.00	0.25	0.50	3.81	0.01	0.27	0.48	4.59	0.00	0.01	0.90
D18	5	7.88	0.00	0.29	0.35	10.13	0.00	0.08	0.65	4.67	0.01	0.56	0.15	9.71	0.01	0.07	0.67	3.52	0.07	0.74	0.06	11.77	0.01	0.01	0.86
D19	4	0.95	0.01	0.49	0.30	0.84	0.01	0.41	0.36	1.54	0.01	0.55	0.26	1.28	0.02	0.80	0.10	-7.34	0.31	0.84	0.08	3.39	0.00	0.03	0.82
D20	4	-0.99	0.01	0.96	0.02	0.73	0.01	0.93	0.03	-6.62	0.02	0.94	0.03	-0.77	0.07	0.95	0.03	-2.70	0.10	0.92	0.04	7.79	-0.01	0.02	0.87
A	22	1.24	0.01	0.46	0.00	1.31	0.01	0.45	0.00	-0.21	0.15	0.52	0.00	0.38	0.05	0.62	0.00	0.50	0.13	0.42	0.00	0.63	0.27	0.46	0.00
DOH	33	0.30	0.01	0.92	0.00	0.14	0.01	0.92	0.00	-0.12	0.22	0.42	0.00	-0.01	0.05	0.93	0.00	-0.44	0.16	0.78	0.00	0.55	0.12	0.32	0.00
WU	25	2.51	0.01	0.72	0.00	2.51	0.01	0.72	0.00	1.29	0.25	0.84	0.00	1.70	0.04	0.78	0.00	-0.16	0.20	0.65	0.00	2.35	0.21	0.69	0.00

Discussion

There are several plausible processes that could connect potential anthropogenic K^+ sources to precipitation collectors. Elevated K^+ in the Kolekole and Schofield Barracks collectors during the 2020 trade wind season could have been sourced from pineapple cultivation areas approximately 8 km to the northeast. These areas are aligned with the predominant trade wind direction. The Haleʻiwa and Mokulēʻia collectors, likewise, are situated southwest of agricultural areas and subject to persistent northeasterly trade winds for much of the year, which could explain elevated NSS K^+ in several samples at these locations (Fig. 7). The Waiʻanae Kai collector (D19) is isolated from trades by Mount Kaʻala, so dust transport from agricultural areas in central and north Oʻahu is unlikely. Non-sea salt K^+ deposition at this site could have been caused by sea breeze wind patterns transporting dust particles from diversified crop areas to the southwest (Fig. 7). Direct contamination was also a possibility at several sites. The Wheeler Army Airfield, Wahiawa, East Range, and Waimano Ridge collectors were all located close to residential or manicured areas. Elevated K^+ at these locations could be due to hand fertilization associated with groundskeeping. Potassium enrichment from non-agricultural sources, such as bird feces or algal residue, is also possible, although this potentiality was not explored in detail. Altogether, the spatiotemporal trends in bulk precipitation chemistry suggest local agricultural dust transportation is a plausible mechanism for non-marine K^+ deposition within the study area.

Sulfate and magnesium

Results

On average, Mg^{2+} and SO_4^{2-} constituted less than 5% and 3% of the measured ion load in bulk precipitation samples. Volume-weighted average SO_4^{2-} ranged from 0.35 ± 0.91 mg L^{-1} at Kaʻala Culvert 49 (K3) to 7.02 ± 1.45 mg L^{-1} at Kaʻena Point (D11). Volume-weighted average Mg^{2+} ranged from 0.34 ± 0.57 mg L^{-1} at Kaʻala Milepost 3 (K2) to 2.96 ± 0.73 mg L^{-1} at Kaʻena Point (D11). Instrumental uncertainties based on duplicate sampling were ± 1.82 mg L^{-1} SO_4^{2-} and ± 0.32 mg L^{-1} Mg^{2+} (Tachera et al., 2021). Sea-salt correction propagated uncertainty was ± 0.33 mg L^{-1} NSS Mg^{2+} and ± 1.83 mg L^{-1} NSS SO_4^{2-}. Marine enrichment factors showed a slight elevation of SO_4^{2-} compared to Mg^{2+}, though both constituents were close to marine major ion ratios.

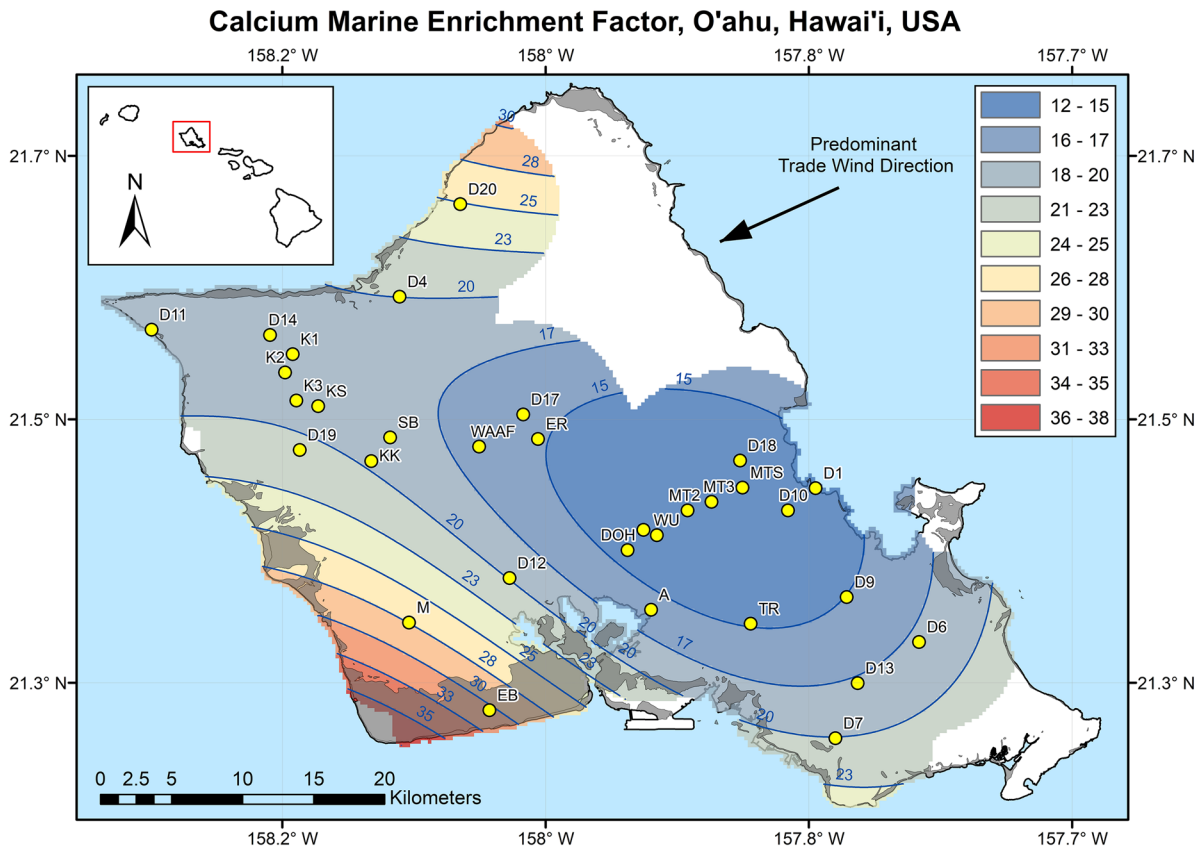

Fig. 5 Calcium marine enrichment factor map for O'ahu, HI, USA, interpolated from bulk precipitation chemistry data collected between March 2017 and June 2021. Data from Dores et al. (2020) are included. The interpolation method was ordinary kriging. Enrichment factor contour intervals are shown in blue. Exposures of calcite-cemented, shallow marine sediments are shown in dark gray. The coverage was interpolated from data at the collector locations displayed. Points were given a 6-km buffer to limit the extent of interpolation

Discussion

Differentiating Mg^{2+} and SO_4^{2-} sources in bulk precipitation was difficult due to low concentrations, relatively high uncertainty, and irregular spatiotemporal patterns. Samples with excess SO_4^{2-} and Mg^{2+} were found most frequently in collectors at lower elevations or in more urbanized areas. Collectors in high elevation and pristine settings had minor SO_4^{2-} and Mg^{2+} and negligible NSS contributions. Regression analysis of rainfall rates (mm day^{-1}) vs. Mg^{2+} and SO_4^{2-} bulk deposition (g ha^{-1} day^{-1}) indicates that both dry and wet depositions occurred (Table 5). Samples from the Ewa Beach (EB) collector showed the most substantial component of NSS Mg^{2+}, accounting for approximately 20% of the total Mg^{2+} ion load. This is potentially related to the collector's downwind proximity to the heavy military and aviation activity centered on Pearl Harbor, which includes Joint Base Pearl Harbor Hickam, and the Daniel K. Inouye International Airport. Elevated NSS Mg^{2+} at Ewa Beach could also be due to dust transport of dolomitized soils. This phenomenon has been observed in semi-arid settings on O'ahu in the past (Sherman et al., 1947). However, it is unclear why similar trends were not observed in other semi-arid locations, including Wai'anae Kai (D19) and Ka'ena Point (D11). Samples from the Makakilo collector (M) showed the most substantial component of NSS SO_4^{2-}, with an average of 40% of the ion load coming from NSS sources. The Kahe Power Plant, approximately 5 km to the east, is a potential source

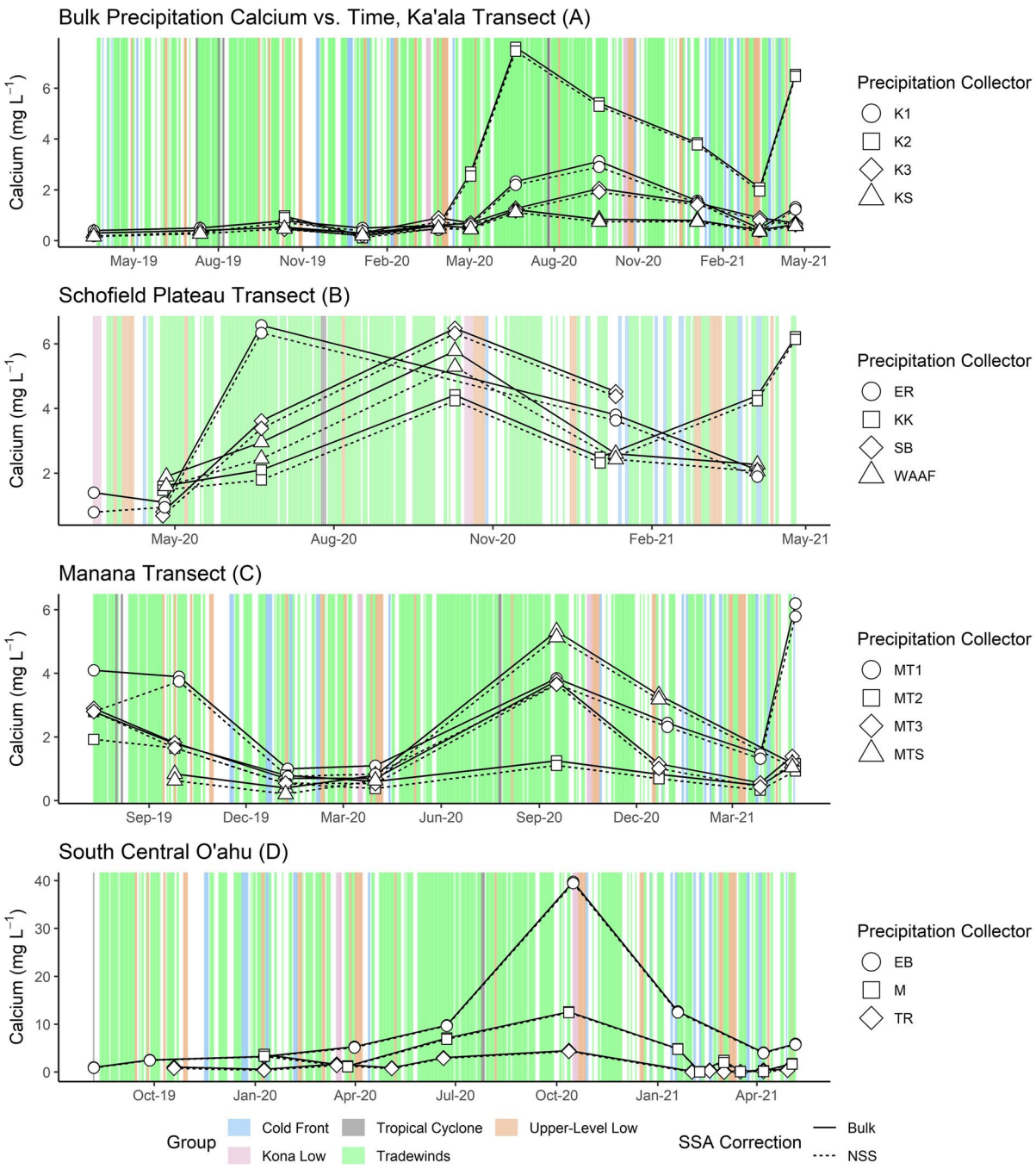

Fig. 6 Time series of bulk precipitation Ca^{2+} concentrations taken on O'ahu, HI, USA. Ka'ala Transect (**A**), Schofield Plateau Transect (**B**), Manana Transect (**C**), and Southcentral O'ahu collectors (**D**). Non-sea salt (NSS) contributions are displayed in dotted lines. Non-sea salt uncertainty was ± 0.66 mg L^{-1}. Weather trend data derived from International Global Radiosonde Archive (IGRA) weather balloon launces at Līhue, Kauai (Durre et al., 2006, 2016), and from monthly weather summaries provided by the National Oceanic and Atmospheric Administration (NOAA/NWS, 2023) are shown in the background

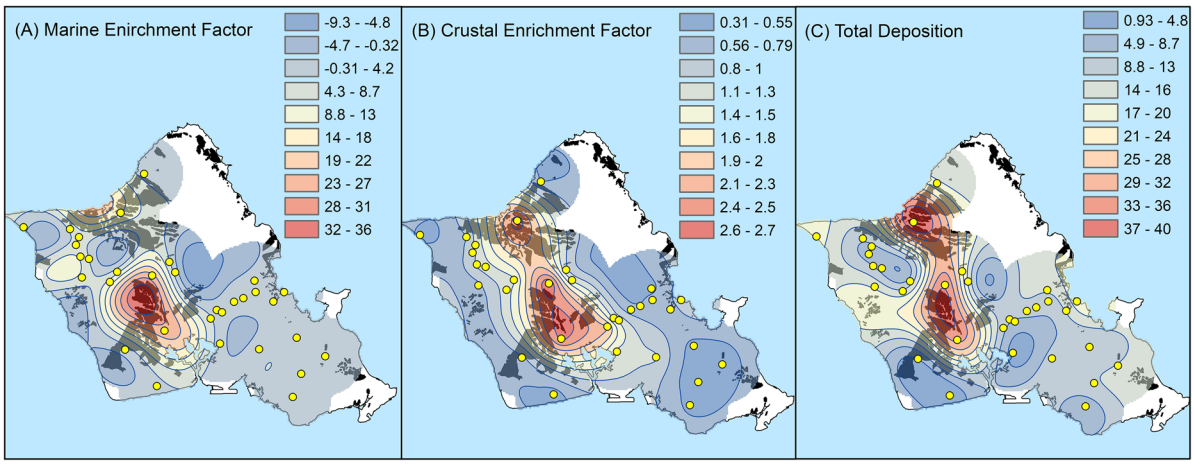

Fig. 7 Interpolated coverages of K^+ marine enrichment factor (**A**), K^+ crustal enrichment factor (**B**), and average annual bulk deposition of K^+ in kilograms per hectare (**C**). The interpolation method was ordinary kriging. Interpolation points are shown in yellow. The interpolated coverages were limited to a 6-km buffer around each point. Data from Dores et al. (2020) are included. The crustal enrichment factor was calculated using Ca^{2+} as the reference species and was based on average crustal composition (Kring, 1997). The marine enrichment factor was calculated using Cl^- as the reference species and was based on average seawater composition (Wilson, 1975). Agricultural areas are shown in black

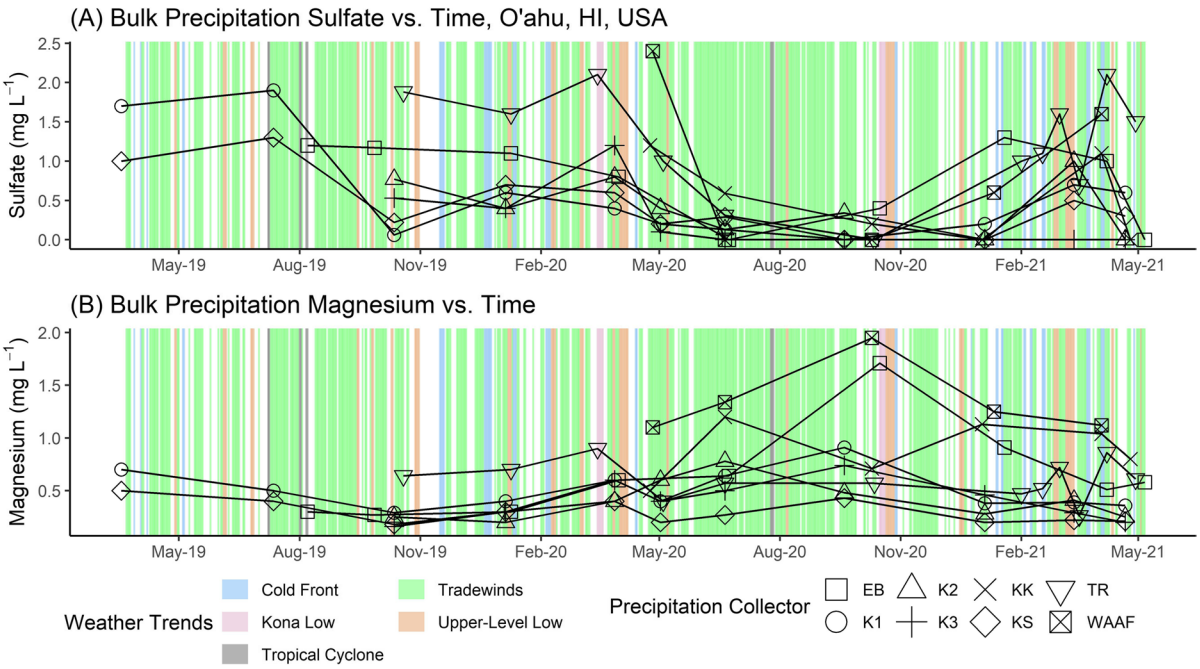

Fig. 8 Time series of bulk precipitation Mg^{2+} and SO_4^{2-} concentrations in bulk precipitation taken on O'ahu, HI, USA, between June 2018 and May 2021. Abbreviations: EB is Ewa Beach, TR is Tripler Ridge, WAAF is Wheeler Army Airfield, KK is Kolekole Pass, and K is Ka'ala. Weather trend data derived from International Global Radiosonde Archive (IGRA) weather balloon launches at Līhue, Kauai (Durre et al., 2006, 2016), and from monthly weather summaries provided by the National Oceanic and Atmospheric Administration (NOAA/NWS, 2023) are shown in the background

of combustion particulate byproducts. However, there was no clear correlation between wind patterns and excess SO_4^{2-} at Makakilo. Volcanic emissions from Kīlauea have been associated with elevated SO_4^{2-} in precipitation on O'ahu in the past (Dugan & Ekern, 1984), but this trend was not observed in this study, likely due to low volcanic activity during the sampling period.

At some locations, Mg^{2+} and SO_4^{2-} had an apparent inverse relationship. Following the 2020 trade wind season, bulk precipitation samples showed elevated Mg^{2+}, and roughly proportional depletion of SO_4^{2-} at EB, Tripler Ridge (TR), Wheeler Army Airfield (WAAF), Kolekole Pass (KK), and all collectors along the Ka'ala transect (K1, K2, K3, and KS) (Fig. 8). This inverse relationship was also visible in the PCA. Principal component 6, which accounted for 0.5% of the total variance in the dataset, shows an eigenvector of −0.56 for SO_4^{2-} and 0.82 for Mg^{2+}, indicating strong inverse loading for these two constituents (Table 4; Abdi & Williams, 2010). The cause of this relationship is unclear but could indicate chemical reactions involving both species, whereby one is enriched relative to the other through a reaction pathway involving both. The trends in Mg^{2+} and SO_4^{2-} concentrations in bulk precipitation do not definitively point to any single source or process for non-marine deposition. Particulate from combustion emissions and marine biogenic activity are the most likely sources of NSS SO_4^{2-}. Aviation activity, leaflitter decay, and local dust transport are the most likely sources of NSS Mg^{2+}.

Conclusions

Analysis of inorganic constituents in precipitation confirms that marine-origin SSAs exert the strongest influence on precipitation major ion chemistry throughout the study area. However, it also illuminates several interesting NSS deposition sources and atmospheric processes that impact precipitation chemistry. The strong correlation between precipitation chloride-to-sodium ratios and the seawater chloride-to-sodium ratio indicates that these ions are sourced almost exclusively from marine-origin SSAs. Sodium concentrations suggest at least one NSS source that is most likely terrestrial dust transported from the Asian continent above the trade wind regime. Chloride was selected as the reference species for SSA corrections due to measurable excess in Na^+ relative to seawater composition. Spatially variable NSS Ca^{2+} concentrations in precipitation suggest that local dust transport, most likely from calcite-rich sedimentary deposits and/or cement production, is the dominant source of NSS Ca^{2+} deposition. Potassium concentrations were generally low, but a number of collectors close to agricultural areas showed accumulations of NSS potassium-rich dust through dry deposition. Sulfate and Mg^{2+} concentrations were low, highly variable, and often inversely related, suggesting a chemical reaction involving both species and making source differentiation difficult. Lastly, the cumulative effect of summing and squaring uncertainties in the volume-weighting calculations produced large errors in some VWA chemical concentrations, indicating increased instrumental precision may be necessary for more comprehensive analysis using this procedure. These findings illuminate some of the key atmospheric processes governing precipitation chemistry in and around the Pearl Harbor aquifer and help to establish a baseline for assessing future fluctuations. Future work will examine spatiotemporal changes in water stable isotopologue concentrations (oxygen-18 and deuterium) within precipitation over the same sampling period and collector distribution. These two efforts aim to characterize precipitation chemistry within the Pearl Harbor region and postulate its primary controlling factors. These two efforts will culminate in an examination of groundwater chemistry within the study area with the ultimate goal of constraining groundwater flow paths by means of natural geochemical tracers.

Appendix. Processes impacting precipitation inorganic chemistry

There are three dominant sources of inorganic ions in precipitation: terrestrial (crustal) dust, marine sea-salt aerosols (SSA), and anthropogenic activity. Terrestrial dust particles accumulate in the atmosphere through weathering of rocks and aeolian transport (Keresztesi et al., 2020; Pearson & Fisher, 1971); sea-salt aerosols are formed when bubbles produced by breaking waves rise to the surface and burst, releasing microscopic aerosol particles which are transported by air currents (Keene et al., 1986; Laskin et al., 2012; Lewis & Schwartz, 2004); and anthropogenic sources of atmospheric inorganic particulates include a great variety of activities with the most massive

sources being combustion of fossil fuels, industrial processes, and agriculture (Keresztesi et al., 2020; Lu et al., 2011; Pearson & Fisher, 1971). Many processes can influence both the speciation and concentration of inorganics in the atmosphere, notably the formation and evolution of sea-salt aerosols, biogenic activity, acid–base reactions, hygroscopicity, and terrestrial dust transport, each of which will be discussed below.

Due to the study area's proximity to the ocean, marine processes must be considered carefully. Though the composition of ocean water varies across the globe, the relative ratios of inorganic ions in seawater are consistent (Keene et al., 1986; Lewis & Schwartz, 2004). One fundamental assumption in assessing bulk precipitation chemistry in coastal and marine environments is that the chemistry of SSAs produced by wave action reflects the chemistry of seawater; that is, the relative ratios of inorganic ions are stable in the process of SSA formation. This assumption is well founded and supported by many years of research (Lewis, 1981; Keene et al., 1986; Skartveit, 1982; Hoffman & Duce, 1972; Khemani et al., 1985; Junge, 1972; Seto et al., 1969).

After SSA formation, there are three critical categories of chemical processes that can impact the relative ratios of inorganics in marine atmospheric moisture: biogenic activity, acid–base reactions, and variations in hygroscopicity among common inorganic salts. Among the ions examined here, SO_4^{2-} is the most important product of biogenic activity. Biogenic SO_4^{2-} is thought to be largely produced through the oxidation of dimethyl sulfide (DMS) into methanesulfonic acid (MSA) through reaction with free radicals (Ghahremaninezhad et al., 2016; Norman et al., 1999; Saltzman et al., 1986), though there are many other possible reaction intermediaries and products. The sources of DMS, and the reaction pathways that connect algae with DMS, remain largely uncharacterized. Gaseous DMS is transported into the atmosphere through turbulent diffusion (Ghahremaninezhad et al., 2016; Hu et al., 2011; Nightingale et al., 2000). Oxidized DMS compounds conglomerate on preexisting particles to become cloud condensation nuclei (CNN), which can then accumulate moisture and intermix with SSAs, enriching marine atmospheric moisture in SO_4^{2-} relative to the seawater ratios (Charlson et al., 1987; Ghahremaninezhad et al., 2016).

Acid–base reactions occurring on the surface of SSAs can also change the chemistry of marine moisture. Chloride is the ion most susceptible to these reactions. Many studies have reported measurable depletion of Cl^- in SSAs because of reaction with inorganic and weak organic acids (Laskin et al., 2012 and references therein). These acids tend to accumulate in the atmosphere near urbanized and industrialized areas similar to much of O'ahu. Confusingly, the reactions driven forward by these acids can produce gaseous hydrochloric acid (HCl), which has been theorized to be a source of Cl^- enrichment in precipitation under certain atmospheric conditions (Keene et al., 1986). Acid–base reactions therefore have the potential to both increase and decrease Cl^- concentrations in SSAs. Neutralization of acidity in precipitation by reaction with terrestrially sourced alkaline species has also been observed (Keresztesi et al., 2020; Lee et al., 2000). These processes are particularly important in completing SSA corrections, which frequently use Cl^- concentrations as the basis for the correction.

The capacity of an aerosol particle to attract and retain moisture can impact the formation of CCN, which can affect when certain chemical species accumulate in precipitation. The tendency of a compound to absorb water on its surface is called hygroscopicity. The hygroscopicity of inorganic salts changes with temperature, humidity, particle size, and species (Hu et al., 2011). The general trend is that when relative humidity (RH) rises above a threshold, known as the deliquescence RH (DRH), the hygroscopicity of inorganic salts, particularly ammonium salts, increases with particle size (Hu et al., 2010, 2011). Conversely, below the DRH, evaporation of ammonium salts is enhanced as RH rises. This can result in measurable enrichment or depletion of major ions in precipitation depending on the specific atmospheric conditions. Chloride and SO_4^{2-} are the most susceptible to hygroscopic processes (Hu et al., 2011). The net effect of these three categories of marine-focused chemical processes is a tendency of SO_4^{2-} and Cl^- concentrations in bulk precipitation chemistry to depart from the seawater ratios. Careful comparison must be made between bulk precipitation chemistry and seawater ratios to assess the magnitude of these effects in coastal and marine settings. This supports the conclusion of Keene et al. (1986) that selecting

a reference species for sea-salt corrections must be done deliberately, based on objective criteria.

Dust transport of terrestrially and anthropogenically derived inorganic constituents can also impact bulk precipitation chemistry. Magnesium, Ca^{2+}, Na^{+}, and K^{+} are among the most abundant elements in the Earth's crust (Kring, 1997). Rock and aeolian transport weathering can disperse substantial quantities of these constituents over vast distances (Chung & Park, 1998). Many studies have linked the presence of Ca^{2+} and Mg^{2+} in precipitation to terrestrial dust transport (Niu et al., 2014; Szép, 2019; Szép et al., 2018; Xiao, 2016; Zhang et al., 2003; Loye-Pilot et al., 1986; Brahney et al., 2013). Biomass burning and potash fertilization have also been linked to elevated K^{+} in bulk precipitation (Keresztesi et al., 2020; Lu et al., 2011). Potassium enrichment of coastal precipitation has also been attributed to high biogenic productivity in the North Sea and Norwegian Sea (Skartveit, 1982).

Several studies have documented the effects of long-range dust transport in the Pacific. Suzuki and Tsunogai (1988) found that a large part of the non-sea-salt (NSS) Ca^{2+} in the troposphere over the western North Pacific originated from arid regions in Asia. Darzi and Winchester (1982) determined that local and continental soils were the only major sources of terrestrial elements in dust aerosols on Hawai'i Island and likewise linked the origin of continental dust to arid regions in Asia. Using trajectory analysis, Shaw (1980) determined that an expansive atmospheric dust plume that passed over Hawai'i from late April to early May 1979 originated in the eastern deserts of Asia. Lee et al. (2000) attributed alkaline dust content in precipitation on the Korean peninsula to long-range transport from desert regions of Asia. They found that local aerosol transport derived from calcite and basalt exposure weathering contributed measurably to precipitation chemistry. Saltzman et al. (1986) studied bulk precipitation chemistry on Midway Atoll and observed significant seasonal trends in continental anthropogenic and marine biogenic NSS SO_4^{2-} deposition. Satake and Yamane (1992) analyzed NSS SO_4^{2-} deposition on central Japan's west coast and linked increased winter deposition to long-range transport from the Asian continent. These, and many other works, demonstrate that terrestrial dust can be a significant source of inorganic nutrients to precipitation in coastal and marine settings.

Acknowledgements The authors wish to express their gratitude to Michael and April Wolfe, the State of Hawai'i Department of Health, the State of Hawai'i Department of Land and Natural Resources, the Schofield Barracks Directorate of Public Works, Mililani High School, and the Ko'olau Mountains Watershed Partnership for land access and sampling assistance. We would also like to express our gratitude to Scott Rowland of the University of Hawai'i at Mānoa for his helpful insights and mentorship through the preparation of this manuscript.

Author contributions CRediT authorship contribution statement - Theodore Brennis: Conceptualization, Methodology; Software, Formal analysis, Investigation, Visualization, Writing â€“ original draft preparation. Nicole Lautze: Conceptualization, Resources, Funding acquisition, Writing â€“ review and editing, Supervision, Project administration. Robert Whittier: Methodology, Investigation, Validation, Writing â€“ review and editing. Giuseppe Torri: Validation, Formal analysis, Writing â€“ review and editing. Donald Thomas: Conceptualization, Writing â€“ review and editing.

Funding This project has been partially funded by the NSF Hawai'i EPSCoR Program through the National Science Foundation's Research Infrastructure Improvement award (RII) Track-1: 'Ike Wai: Securing Hawai'i's Water Future Award # OIA-1557349. G.T. and is supported by NSF Grant AGS-1945972. The project was also funded by the Department of Defense (DoD) Science, Mathematics and Research for Transformation (SMART) Service-for-Scholarship program. NSF Hawai'i EPSCoR Program Research Infrastructure Improvement award (RII) Track-1: 'Ike Wai: Securing Hawai'i's Water Future Award # OIA-1557349. G.T.,NSF Grant AGS-1945972,NSF Grant AGS-1945972

Data availability The data that support the findings of this study are openly available at: https://doi.org/10.5281/zenodo.7838359.

Code availability The R code used to carry out the calculations and prepare the figures is also available by request to the corresponding author.

Declarations

All authors have read, understood, and have complied as applicable with the statement on "Ethical responsibilities of Authors" as found in the Instructions for Authors.

Ethics approval Not applicable.

Consent to participate Not applicable.

Consent for publication Not applicable.

Competing interest Not applicable.

References

Abdi, H., & Williams, L. (2010). Principal component analysis. *Wiley Interdisciplinary Reviews. Computational Statistics, 2*(4), 433–459. https://doi.org/10.1002/wics.101

Akpo, A., Galy-Lacaux, C., Laouali, D., Delon, C., Liousse, C., Adon, M., & Darakpa, C. (2015). Precipitation chemistry and wet deposition in a remote wet savanna site in West Africa: Djougou (Benin). *Atmospheric Environment, 115*, 110–123. https://doi.org/10.1016/j.atmosenv.2015.04.064

Booth, H., Lautze, N., Tachera, D., & Dores, D. (2021). Event-based stable isotope analysis of precipitation along a high resolution transect on the south face of O'ahu, Hawai'i. *Pacific Science*, *75*(3), 421–441B. https://doi.org/10.2984/75.3.9

Brahney, J., Ballantyne, A., Sievers, C., & Neff, J. (2013). Increasing Ca2+ deposition in the wester US: The role of mineral aerosols. *Aeolian Research, 10*, 77–87. https://doi.org/10.1016/j.aeolia.2013.04.003

Cao, G., Giambelluca, T., Stevens, D., & Schroeder, T. (2007). Inversion variability in the Hawaiian trade wind regime. *Journal of Climate, 20*(7), 1145–1160. https://doi.org/10.1175/JCLI4033.1

Charlson, R., Lovelock, J., Andreae, M., & Warren, S. (1987). Oceanic phytoplankton, atmospheric sulphur, cloud albedo and climate. *Nature, 326*, 655–661.

Chung, K., & Park, S. (1998). A numerical study on the size and deposition of yellow sand events. *Journal of Korea Air Pollution Research Association, 10*, 64–72.

Darzi, M., & Winchester, J. (1982). Resolution of basaltic and continental aerosol components during spring and summer within the boundary layer of Hawaii. *Journal of Geophysical Research, 87*(C9), 7262–7272.

Dores, D., Glenn, C. R., Torri, G., Whittier, R. B., & Popp, B. (2020). Implications for groundwater recharge from stable isotopic composition of precipitation in Hawai'i during the 2017–2018 La Niña. *Hydrological Processes, 34*(24), 4675–4696. https://doi.org/10.1002/hyp.13907

Dugan, G., & Ekern, P. (1984). *Chemical constituents of rainfall at different locations on O'ahu, Hawai'i.* University of Hawai'i at Mānoa. Honolulu: Water Resources Research Center.

Durre, I., Vose, R., & Wuertz, D. (2006). Overview of the integrated global radiosonde archive. *Journal of Climate, 19*(1), 53–68. https://doi.org/10.1175/JCLI3594.1

Durre, I., Xungang, Y., Vose, R., Applequist, S., & Arnfield, J. (2016). Integrated Global Radiosonde Archive (IGRA), version 2. *Subset USM00091165, Lihue, HI, USA*. NOAA National Centers for Environmental Information. https://doi.org/10.7289/V5X63K0Q

Fackrell, J. K., Glenn, C. R., Thomas, D., Whittier, R., & Popp, B. (2020). Stable isotopes of precipitation and groundwater provide new insight into groundwater recharge and flow in a structurally complex hydrogeologic system: West Hawai'i, USA. *Hydrogeology Journal, 28*(4), 1191–1207. https://doi.org/10.1007/s10040-020-02143-9

Fletcher, C. H., Bochicchio, C., Conger, C. L., Engels, M. S., Feirstein, E. J., Frazier, N., Glenn C. R., Grigg R. W., Grossman, E. E., Harney, J. N., & Isoun E. (2008). Geology of Hawaii Reefs. In *Coral Reefs of the USA* (pp. 435–487). Springer Netherlands. https://doi.org/10.1007/978-1-4020-6847-8_11

Frazier, A., & Giambelluca, T. (2017). Spatial trend analysis of Hawaiian rainfall from 1920 to 2012. *International Journal of Climatology*, 37(5), 2522–2531. https://doi.org/10.1002/joc.4862

Ghahremaninezhad, R., Norman, A.-L., Abbatt, J., Levasseur, M., & Thomas, J. (2016). Biogenic, anthropogenic and sea salt sulfate size-segregated aerosols in the Arctic summer. *Atmospheric Chemistry and Physics, 16*(8), 5191–5202. https://doi.org/10.5194/acp-16-5191-2016

Giambelluca, T. (1983). *Water balance of the Pearl Harbor-Honolulu Basin, Hawai'i, 1946–1975.* Water Resources Research Center, University of Hawai'i at Manoa.

Giambelluca, T., Chen, Q., Frazier, A., Price, J., Chen, Y.-L., Chu, P.-S., & Delparte, D. (2013). Online Rainfall Atlas of Hawai'i: Bulletin of the American Meteorological Society. v. *94*, 313–316. https://doi.org/10.1175/BAMSD-11-00228.1

Glenn, C., Whittier, R., Dailer, M., El-Kadi, A., Fackrell, J., Kelly, J., & Sevadjian, J. (2013). *Lahaina Groundwater Tracer Study - Lahaina, Maui, Hawaii.* Final report prepared for the State of Hawaii Department of Health, the U.S. Environmental Protection Agency, and the U.S. Army Engineer Research and Development Center.

Harding, D., & Miller, J. (1982). The influence on rain chemistry of the Hawaiian Volcano Kilauea. *Journal of Geophysical Research, 87*(C2), 1225–1230.

Hautman, D., & Munch, D. (1997). *Method 300.1, revision 1–0: Determination of inorganic anions in drinking water by ion chromatography.* U.S. Environmental Protection Agency, National Exposure Research Laboratory, Office of Research and Development, Cincinnati OH.

Hoffman, G., & Duce, R. (1972). Consideration of the chemical fractionation of alkali and alkaline earth metals in the Hawaiian marine atmosphere. *Journal of Geophysical Research, 77*(27), 5161–5169. https://doi.org/10.1029/JC077i027p05161

Hu, D., Chen, J., Ye, X., Li, L., & Yang, X. (2011). Hygroscopicity and evaporation of ammonium chloride and ammonium nitrate: Relative humidity and size effects on the growth factor. *Atmospheric Environment (1994), 45*(14), 2349–2355. https://doi.org/10.1016/j.atmosenv.2011.02.024

Hu, D., Qiao, L., Chen, J., Ye, X., Yang, X., Cheng, T., & Fang, W. (2010). Hygroscopicity of inorganic aerosols: Size and relative humidity effects on the growth factor. *Aerosol and Air Quality Research, 10*, 255–264.

Hutchinson, G. (1954). The Solar System: The biochemistry of the terrestrial atmosphere. In G. Kuiper (Ed.), *The Eart as a Planet* (Vol. 2, pp. 371–433). University of Chicago Press.

Junge, C. (1972). Our knowledge of the physico-chemistry of aerosols in the undisturbed marine environment. *Journal of Geophysical Research, 77*(27), 5183–5200. https://doi.org/10.1029/JC077i027p05183

Keene, W., Pszenny, A. A., Galloway, J., & Hawley, M. (1986). Sea-salt corrections and interpretation of constituent ratios in marine precipitation. *Journal of Geophysical Research, 91*(D6), 6647–6658. https://doi.org/10.1029/JD091iD06p06647

Keresztesi, Á., Nita, I.-A., Boga, R., Birsan, M.-V., Bodor, Z., & Szép, R. (2020). Spatial and long-term analysis of rainwater chemistry over the conterminous United States. *Environmental Research, 188*, 109872–109872. https://doi.org/10.1016/j.envres.2020.109872

Khemani, L., Momin, G., Naik, M., Prakasa Rao, P., Kumar, R., & Ramana Murty, B. (1985). Trace elements and sea salt aerosols over the sea areas around the Indian subcontinent. *Atmospheric Environment, 19*(2), 277–284. https://doi.org/10.1016/0004-6981(85)90095-2

Kring, D. A. (1997). Composition of Earth's continental crust as inferred from the compositions of impact melt sheets. *Lunar and Planetary Science XXVIII; 28th Lunar and Planetary Science Conference*, (pp. 763-). Houston, TX.

Kroopnick, P. (1977). The SO4: Cl ratio in oceanic rainwater. *Pacific Science, 31*(1), 91–106.

Laskin, A., Moffet, R. C., Gilles, M. K., Fast, J. D., Zaveri, R. A., Wang, B., & Shutthanandan, J. (2012). Tropospheric chemistry of internally mixed sea salt and organic particles: Surprising reactivity of NaCl with weak organic acids. *Journal of Geophysical Research. D. (Atmospheres), 117*(D15). https://doi.org/10.1029/2012JD017743

Lee, B., Hong, S., & Lee, D. (2000). Chemical composition of precipitation and wet deposition of major ions on the Korean peninsula. *Atmospheric Environment, 34*, 563–575.

Lewis, E., & Schwartz, S. (2004). *Sea salt aerosol production: mechanisms, methods, measurements, and models - A critical review.* Washington D.C.: American Geophyscial Union.

Lewis, W. M. (1981). Precipitation chemistry and nutrient loading by precipitation in a tropical watershed. *Water Resources Research (united States), 17*(1), 169–181. https://doi.org/10.1029/WR017i001p00169

Li, C., Kang, S., Zhang, Q., & Kaspari, S. (2007). Major ionic composition of precipitation in the Nam Co region. *Central Tibetan Plateau. Atmospheric Research, 85*(3), 351–360. https://doi.org/10.1016/j.atmosres.2007.02.006

Longman, R., Ellison, T., Giambelluca, T., & Kaiser, L. (2021). A 20-year analysis of disturbance-driven rainfall on O'ahu, Hawai'i. *Monthly Weather Review*. https://doi.org/10.1175/MWR-D-20-0287.1

Loye-Pilot, M., Martin, J., & Morelli, J. (1986). Influence of Saharan dust on the rain acidity and atmospheric input to the Mediterranean. *Nature, 321*, 427–428.

Lu, X., Li, L. Y., Li, N., Yang, G., Luo, D., & Chen, J. (2011). Chemical characteristics of spring rainwater of Xi'an city, NW China. *Atmospheric Environment (1994), 45*(28), 5058–5063. https://doi.org/10.1016/j.atmosenv.2011.06.026.

Manahan, S. (2017). *Environmental chemistry.* (10, Ed.) Boca Raton, FL: CRC Press.

Miller, J., & Yoshinaga, A. (1981). The pH of Hawaiian precipitation: A preliminary report. *Geophyscial Research Letters, 8*(7), 779–782.

Mphepya, J., Pienaar, J., Galy-Lacaux, C., Held, G., & Turner, C. (2004). Precipitation chemistry in semiarid areas of Southern Africa: A case study of a rural and an industrial site. *Journal of Atmospheric Chemistry, 47*(1), 1–24.

Neff, J., Belnap, R., & Lamothe, P. (2005). Multi-decadal impacts of grazing on soil physical and biogeochemical properties in southeast Utah. *Ecological Applications, 15*(1), 87–95.

Nightingale, P., Liss, P., & Schlosser, P. (2000). Measurements of air-sea gas transfer during an open ocean algal bloom. *Geophysical Research Letters, 27*, 2117–2120.

Niu, H., He, Y., Lu, X., Shen, J., Du, J., & Zhang, T.,... Chang, L. (2014). Chemical composition of rainwater in the yulong snow mountain region, southwestern China. *Atmospheric Reserach, 144*, 195–206. https://doi.org/10.1016/j.atmosres.2014.03.010

NOAA/NWS. (2023). *Hawaii monthly weather summaries.* Retrieved from https://www.hawaii.edu/climate-data-portal/publications-list/?collection_id=PZN8C7R9&collection_name=-%2520NOAA%252FNWS%2520Monthly%2520Precipitation%2520Summaries

Noguchi, Y. (1979). Deformation of trees in Hawaii and its relation to wind. *The Journal of Ecology, 67*(2), 611–628. https://doi.org/10.2307/2259116

Norman, A., Barrie, L., Toom-Sauntry, D., Sirois, A., Krouse, H., Li, S., & Sharma, S. (1999). Sources of aerosol sulfphate at alert: Apportionment using stable isotopes. *Journal of Geophysical Research, 104*, 11619–11631.

Pearson, F., & Fisher, D. W. (1971). *Chemical composition of atmospheric precipitation in the Northeastern United States.* U.S. Geological Survey, U.S. Department of the Interior. https://doi.org/10.3133/wsp1535P

Pilson, M. E. (1998). *An introduction to the chemistry of the sea* (2nd ed.). Cambridge University Press.

Saltzman, E., Savoie, D., Prospero, J., & Zika, R. (1986). Methanosulfonic acid and non-sea-salt sulfate in Pacific air: Ragional and seasonal variations. *Journal of Atmospheric Chemistry*, 277–240.

Satake, H., & Yamane, T. (1992). Deposition of non-sea salt sulfate observed at Toyama facing the Sea of Japan for the period of 1981–1991. *Geochemical Journal, 26*, 299–305.

Scholl, M., & Ingebritsen, S. (1995). *Total and non-seasalt sulfate and chloride measured in bulk precipitation samples from the Kilauea Volcano area, Hawaii.* U.S. Geological Survey, U.S. Department of Interior. Retrieved from https://pubs.usgs.gov/wri/1995/4001/report.pdf

Scholl, M. A., Gingerich, S. B., & Tribble, J. W. (2002). The influence of microclimates and fog on stable isotope signatures used in interpretation of regional hydrology: East Maui. *Hawaii. Journal of Hydrology (amsterdam), 264*(1), 170–184. https://doi.org/10.1016/S0022-1694(02)00073-2

Seto, Y., Duce, R., & Woodcock, A. (1969). Sodium-to-chlorine ratio in Hawaiian rains as a function of distance inland and of elevation. *Journal of Geophysical Research, 74*(4), 1101–1103. https://doi-org.eres.library.manoa.hawaii.edu/10.1029/JB074i004p01101

Shaw, G. (1980). Transport of Asian desert aerosol to the Hawaiian Islands. *Journal of Applied Meteorology, 19*, 1254–1259.

Sherman, G., Kanehiro, Y., & Fujimoto, C. (1947). Dolomitization in semi-arid Hawaiian soils. *Pacific Science*.

Sherrod, D., Sinton, J., Watkins, S., & Brunt, K. (2021). *Geologic map of the State of Hawai'i: U.S.Geological Survey Scientific Investigations Map 3143, pamphlet 72 p., 5 sheets, scales 1:100,000 and 1:250,000.*https://doi.org/10.3133/sim3143

Shi, G.-L., Li, X., Feng, Y.-C., Wang, Y.-Q., Wu, J.-H., Li, J., & Zhu, T. (2009). Combined source apportionment, using positive matrix factorization–chemical mass balance and principal component analysis/multiple linear regression–chemical mass balance models. *Atmospheric Environment, 1994*, 2929–2937. https://doi.org/10.1016/j.atmosenv.2009.02.054

Skartveit, A. (1982). Wet scavenging of sea-salts and acid compounds in a rainy, coastal area. *Atmospheric Environment, 16*(11), 2715–2724.

Suzuki, T., & Tsunogai, S. (1988). Origin of calcium in aerosols over the Western North Pacific. *Journal of Atmospheric Chemistry, 6*, 363–374.

Szép, R., Mateescu, E., Niță, I.-A., Birsan, M.-V., Bodor, Z., & Keresztesi, Á. (2018). Effects of the Eastern Carpathians on atmospheric circulations and precipitation chemistry from 2006 to 2016 at four monitoring stations (Eastern Carpathians, Romania). *Atmospheric Research, 214*, 311–328. https://doi.org/10.1016/j.atmosres.2018.08.009

Szép, R. B. (2019). Influence of peat fires on the rainwater chemistry in intra-mountain basins with specific atmospheric circulations (Eastern Carpathians, Romania). *Science of the Total Environment, 647*, 275–289. https://doi.org/10.1016/j.scitotenv.2018.07.462

Tachera, D., Lautze, N., Torri, G., & Thomas, D. (2021). Characterization of the isotopic composition and bulk ion deposition of precipitation from Central to West Hawai'i Island between 2017 and 2019. *Journal of Hydrology. Regional Studies*, *34*, 100786. https://doi.org/10.1016/j.ejrh.2021.100786

Torri, G., Nugent, A., & Popp, B. (2023). The isotopic composition of rainfall on a subtropical mountainous island. *Journal of Hydrometeorology*. https://doi.org/10.1175/JHM-D-21-0204.1

Wickam, H., Chang, W., Henry, L., Pedersen, T., Takahashi, K., Wilke, C., & Dewey, H. (2016). *Rug plots in the margins*. (S.-V. N. York, Producer) retrieved from ggplot2: Elegant graphics for data analysis. https://ggplot2.tidyverse.org/reference/geom_rug.html

Wilson, T. (1975). Salinity and the major elements of sea water. In J. Riley & G. Skirrow (Eds.), *Chemical oceanography* (2nd ed., Vol. 1, pp. 365–413). Academic.

Xiao, J. (2016). Chemical composition and source identification of rainwater constituents at an urban site in Xi'an. *Environmental Earth Sciences, 75*, 1–12. https://doi.org/10.1007/s12665-015-4997-z

Zhang, D., Peart, M., Jim, C., He, Y., Li, B., & Chen, J. (2003). Precipitation chemistry of Lhasa and other remote towns. *Tibet. Atmospheric Environment, 37*(2), 231–240.